Aβ43 levels determine the onset of pathological amyloid deposition

Marc D. Tambini
UMDNJ New Jersey Medical School: Rutgers New Jersey Medical School
Tao Yin
UMDNJ New Jersey Medical School: Rutgers New Jersey Medical School
Metin Yesiltepe
UMDNJ New Jersey Medical School: Rutgers New Jersey Medical School
Lionel Breuillaud
Biospective, Inc.
Simone P. Zehntner
Biospective, Inc.
Luciano D'Adamio (luciano.dadamio@rutgers.edu)
Rutgers The State University of New Jersey https://orcid.org/0000-0002-2204-9441

Research Article

Keywords: APP - amyloid precursor protein, Presenilin, γ-secretase, Amyloid-β, Alzheimer's disease, Knock–In rat, Amyloid plaques

Posted Date: December 12th, 2022

DOI: https://doi.org/10.21203/rs.3.rs-2272441/v1

Abstract

Background

While most Alzheimer's disease cases are sporadic with late onset (LOAD), ~ 2% of cases are inherited, have an early onset, and are caused by mutations in *Presenilins (PSEN1/2)* or *Amyloid-β Precursor Protein (APP*) genes (familial AD, FAD). PSEN1/2 are the catalytic component of γ-secretase, a protease that generates Aβ peptides of different length from APP. Aβ peptides are the major components of amyloid plaques, a pathological lesion that characterizes AD. Analysis of mechanisms by which PSEN1/2 and APP mutations affect Aβ peptide compositions lead to the implication of the absolute or relative increase in Aβ42 levels in amyloid-β plaques formation and AD pathogenesis. The age at onset of FAD depends on the mutation and can differ by decades, suggesting a link between age at onset of dementia and the effects of distinct FAD mutations on Aβ species profiles. It is reasonable to presume that Aβ peptide compositions that initiate amyloid pathology and disease in FAD patients can also inform about disease mechanisms driving the more common LOAD cases.

Methods

Here, to elucidate the formation of pathogenic Aβ cocktails leading to amyloid pathology, we utilized rat knock-in models of FAD carrying the Swedish *APP* (*App*^{s} allele) and the *PSEN1 L435F* (*Psen1*^{LF} allele) mutations. To accommodate the possibility of differences in pathogenicity of rodent and human Aβ, these rat models are genetically engineered to express human Aβ species as both the Swedish mutant allele and the wild-type rat allele (called *App*^{h}) have been humanized in the Aβ-coding region.

Results

Analysis of the 8 possible FAD mutant permutations demonstrates correlations between mutation-driven alterations in Aβ profiles and amyloid pathology, and indicates that the CNS levels of Aβ43, rather than absolute or relative increases in Aβ42, determine the onset of pathological amyloid deposition.

Conclusions

This study corroborates the critical pathological importance of alterations in the Aβ peptides composition, helps clarifying the molecular determinants initiating amyloid pathology, and supports therapeutic interventions targeting Aβ43 to prevent, delay, or revert AD.

Introduction

Familial forms of Alzheimer's disease (FAD) are caused by mutations in the *Amyloid-β precursor protein* (*APP*) and *Presenilin 1/2* (*PSEN1/2*) genes. APP processing can result in the formation of amyloid β (Aβ). PSEN1/2 are the catalytic components of the γ-secretase complex, a protease that cleaves Aβ from APP-βCTF, a polypeptide generated by β-secretase processing of APP. Aβ peptides of different lengths are generated by two γ-secretase-dependent product lines consisting of 4 sequential COOH→NH2-terminal trimming steps. In the 1st catalytic step, APP-βCTF is processed by γ-secretase at two ε-sites generating two membranes bound Aβ fragments (Aβ49, product line 1, and Aβ48, product line 2). Aβ49 is converted into Aβ46 (2nd catalytic step), which is converted into Aβ43 (3rd catalytic step). Finally, Aβ43 is trimmed into Aβ40 (4th catalytic step). In product line 2, catalytic steps 2–4 originate the following peptides from Aβ48: → Aβ45 → Aβ42 → Aβ38 [1]. The efficiency of these catalytic events depends on the activity and processivity of γ-secretase, and reduced processivity can lead to increased production of longer Aβ peptides at the cost of shorter Aβ species.

The widely accepted amyloid cascade hypothesis postulates that accumulation of Aβ42, which has higher hydrophobicity and is more prone to aggregation than Aβ40, in oligomeric forms and amyloid plaques is the main pathogenic trigger of Alzheimer's disease (AD)[2]. The genetic evidence from FAD cases, i.e., that FAD mutations are found in the genes coding for the Aβ precursor substrate and an Aβ generating protease, is consistent with a pathogenic role of Aβ. The evidence that *APP* and *PSEN1/2* pathogenic mutations alter Aβ production, further supports the amyloid cascade hypothesis. For instance, a double pathogenic mutation in APP, occurring in a Swedish family, just NH_2-terminal to the β-secretase cleavage site, favors β-processing of APP and production of APP-βCTF, causes a strong increase of Aβ generation in humans [3] as well as knock-in mouse [4] and rat [5] models. In contrast, a genetic variant just carboxyl-terminal to the β-site that reduces β-processing of APP and, consequently, reduces Aβ generation in humans [6] and in a knock-in rat model [7], protects against AD [6]. *PSEN1* and *PSEN2* mutations reduce the activity and processivity of γ-secretase [8], leading to an alteration of the ratios between short and long forms of Aβ, in favor of long Aβ forms [9, 10].

In this pathogenic framework, understanding the essential changes in the molecular composition of Aβ profiles that initiate amyloid pathology in AD could point to the Aβ species that should be therapeutically targeted to delay, prevent, or revert amyloid pathology. Most studies have analyzed changes in Aβ42 and/or Aβ40 production, pointing to either absolute or relative (to Aβ40) increments in Aβ42 levels as a pathogenic hallmark in AD [10–19]. Still, few studies have come to opposite conclusions [20, 21]. These contradictions may be the result of a narrow focus on Aβ40 and Aβ42, since FAD mutations can significantly alter the generation of other Aβ species, such as Aβ38 and Aβ43 [8, 22–25].

Model organisms expressing FAD mutations in a physiological manner could help dissect mixtures of Aβ species that favor amyloid pathology. To test this hypothesis, we have utilized two rat knock-in models of FAD. One model carries the aforementioned Swedish *APP* mutation (App^{s} rat) [5]; the other carries the *PSEN1 L435F* mutation ($Psen1^{LF}$ rat) [26]. To accommodate the possibility of differences in pathogenicity of rodent and human Aβ, these rat models are genetically engineered to express human Aβ species as both the Swedish mutant allele and the wild-type rat allele (called App^{h}) have been humanized

in the Aβ-coding region. *App*^{s} knock-in rats recapitulate the biochemical changes of human APP-Swedish metabolism [3, 27, 28] and produce significantly higher levels of human Aβ38, Aβ40 and Aβ42 [5]. Consistent with *in vitro* and *in vivo* evidence [16, 23, 24, 29], the *PSEN1 L435F* mutation causes a significant loss of γ-secretase activity and processivity in rats. *Psen1*^{LF} rats reproduced previously reported alterations in Aβ species [24, 30], which include a reduction in total amyloid production with minimal levels of Aβ38 and Aβ40, while concentrations of Aβ43 are significantly increased [26]. Given the genetic and biochemical faithfulness of these knock-in models to human FAD cases, and the distinct alterations in Aβ species caused by the two pathogenic mutations, in this study, we tested the compound effects of these mutations with the purpose of gaining insights into the composition of pathogenic Aβ cocktails leading to amyloid pathology.

Material And Methods

Experimental animals. All experiments were done according to policies on the care and use of laboratory animals of the Ethical Guidelines for Treatment of Laboratory Animals of the NIH. Relevant protocols were approved by the Rutgers Institutional Animal Care and Use Committee (IACUC) (Protocol #201702513). All efforts were made to minimize animal suffering and reduce the number of rats used.

Rat genotyping. The genotype of rats was verified by DNA sequencing of genomic DNA PCR products as previously reported [5, 26]. To prepare genomic DNA, tail tissue was digested in 300 µl lysis buffer (100mM Tris, 5mM EDTA, 0.2% SDS, 200mM NaCl, pH 8.0) plus 3 µl of 20 µg/ml protease K at 55^{0} C overnight. One hundred µl of a 7.5M Ammonium Acetate solution was added to each sample to precipitate protein, samples were mixed by vortexing for 30 seconds and centrifuged at 15000 x g for 5 min. Supernatant was mixed with 300 µl Isopropanol and centrifuged at 15000 xg for 5 min. to precipitate genomic DNA. The DNAs pellet was desalted with 70% ETOH and was dissolved in water for PCR and sequencing.

Immunohistochemistry (IHC). Rat brain tissue was fixed and stored in 70% ethanol after transcardiac perfusion with PBS and 4% paraformaldehyde fixative. All tissues were dehydrated through graded ethanol and xylene, infiltrated with paraffin wax, and embedded in paraffin blocks. Sections were cut on a rotary microtome at the thickness of 5 µm, floated on a water bath and mounted on glass slides. Slides were manually deparaffinized and rehydrated before the automated IHC. Slides initially underwent antigen retrieval, by one of the following methods, heat-induced epitope-retrieval (HIER) or formic acid (FA) treatment. HIER was performed by incubation in a citrate buffer (pH 6.0) (Abcam, ab93678) and heating to 100 °C for a period of 60 min. FA treatment was a 10-min incubation in 80% FA (Sigma, F0507), followed by washing in tris-buffered saline-Tween 20. All IHC studies were performed at room temperature on a Lab Vision Autostainer 360 (Thermo). Briefly, slides were incubated sequentially with hydrogen peroxide for 5 min, to quench endogenous peroxidase, followed by 5 min in a protein block (Abcam, ab156024), and then incubated with primary antibodies (see Table 1) in antibody diluent (Abcam, ab64211). Antibody binding was amplified using the appropriate secondary reagents (Jackson) (20 min), followed by a horseradish peroxidase conjugate (Jackson) (20 min), and visualized using the

aminoethyl carbazole chromogen (Abcam, ab64252) (20 min). All IHC sections were counterstained with Acid Blue 129 (Sigma, 306496) and mounted with an aqueous mounting medium.

Modified Bielshowski Silver Staining. The slides were manually deparaffinized and re-hydrated prior to histological staining. Rehydrated tissue was immersed in preheated silver nitrate solution (40^{o}C) for 15 min, followed by a deionized water rinse and an incubation in ammoniacal silver solution at 40^{o}C for 10 min (American Master Tech, CA). Silver deposition was performed in the developer solution for a period of 15 min, once a golden brown tissue stain was achieved; the development was stopped by sequential incubations in ammonium water then 5% sodium thiosulfate (American Master Tech, CA). The stained tissue sections were dehydrated in xylene, and mounted in Permount (VWR, Mississauga, Ontario) and coverslipped.

Qualitative image analysis of IHC Sections. The IHC and histology slides were digitized using an Axio Scan.Z1 digital whole slide scanner (Carl Zeiss, Toronto, ON, Canada). The images underwent quality control (QC) review and final images transferred to the Biospective server for qualitative image analysis. All qualitative assessments were performed blinded to the tissue genotype

Rats brain proteins preparation and ELISAs. These procedures were performed as previously described [26, 47–51]. For brain protein preparations, rats were anesthetized with isoflurane and perfused via intracardiac catheterization with ice-cold PBS. Brains were extracted and homogenized with a glass-teflon homogenizer in 250 mM Sucrose, 20 mM Tris-base pH 7.4, 1 mM EDTA, 1mM EGTA plus protease and phosphatase inhibitors (ThermoScientific). All steps were carried out on ice. Homogenates were solubilized with 1% NP-40 for 30 min rotating and spun at 20,000 g for 10 minutes. Supernatants were collected and protein content was quantified by Bradford.

Aβ38, Aβ40 and Aβ42 were measured with V-PLEX Plus Aβ Peptide Panel 1 6E10 (K15200G). Measurements were performed according to the manufacturer's recommendations. Plates were read on a MESO QuickPlex SQ 120. For analysis of Aβ43, IBL Human Amyloidβ (1–43) (FL) Assay Kit (27710) was used according to the manufacturer's recommendations.

Statistical analysis. Data were analyzed using GraphPad Prism software and expressed as mean ± s.e.m. Statistical tests used to evaluate significance and statistical data are shown in Fig. legends. Significant differences were accepted at $P < 0.05$.

Results

Knock-in rats harboring App^{s} **mutant alleles plus one** Psen1^{LF} **allele do not develop amyloid pathology at 18 months of age.** *App^{s}* and *Psen1^{LF}* knock-in rats recapitulate the changes in APP processing and human Aβ production caused by these pathogenic mutations in patients. *App^{s}* rats generate significantly higher levels of APP-βCTF and, consequently, of its γ-cleavage products Aβ peptides [5]. In contrast, *Psen1^{LF}* knock-in rats generate high levels of Aβ43 but minimal levels of Aβ38 and Aβ40, with a reduction

in total amyloid production [26], confirming that this FAD mutation causes a significant loss of γ-secretase activity and processivity. For both knock-in lines, changes in Aβ species are gene-dosage-dependent. To determine whether interactions of these two pathogenic mutations prompt amyloid-β pathology, we crossed $App^{s/h}$:$Psen1^{LF/w}$ to $App^{s/h}$:$Psen1^{w/w}$ rats to generate $App^{h/h}$:$Psen1^{w/w}$ (our control group, 2 males and 2 females), heterozygous and homozygous Swedish ($App^{s/h}$:$Psen1^{w/w}$ and $App^{s/s}$:$Psen1^{w/w}$, 2 males and 2 females for each genotype) double heterozygous ($App^{s/h}$:$Psen1^{LF/w}$, 2 males and 2 females) Swedish homozygous and $Psen1^{LF}$ heterozygous ($App^{s/s}$:$Psen1^{LF/w}$, 3 males and 1 female) rats. Brains were harvested from ~ 18 month-old rats and analyzed by immunohistochemistry (IHC). H&E staining was utilized to assess the tissue quality and overall brain structure. NeuN staining was used to assess neuronal density in the cortical mantle and neuronal cell layers in the hippocampus. GFAP staining was used to assess the activation level of the astrocytes and the presence of neuroinflammation. Iba1 staining was used to assess the activation state of microglia and the potential presence of inflammatory foci. The 6E10 and 4G8 antibodies, which target amino acids 1–17 and 18–23 of Aβ, respectively, were mixed and used to evaluate amyloid plaques. Tau phosphorylation was evaluated with the AT8 antibody. Representative images of dorsal hippocampus and sensory cortex, and of magnified area of the CA1 are shown in Fig. 1a and 1b, respectively.

H&E staining illustrates very similar structures within these brain regions for all knock-in animals (Fig. 1a and 1b). Like the observations made with the H&E-stained sections, no overt neuronal loss was observed with NeuN staining (Fig. 1a and 1b). In GFAP staining, no dense clusters of astrocytes were apparent in 18-month-old knock-in rat, and an even distribution of GFAP expression was observed throughout the brain (Fig. 1a and 1b). Overall, there is no evidence of a widespread astrocytic inflammatory response related to the genotype. Iba1 staining showed no evidence of a clear microglial inflammatory response related to the genotype, i.e., a feature consistent in most of the samples of the group (Fig. 1a and 1b). Throughout the brain, the morphology of the microglia is generally ramified, without patches of bushy activated microglia or inflammatory foci and both female and male cohorts have very similar Iba1 staining patterns. The 6E10 + 4G8 antibodies did not show any sign of amyloid pathology in these 18-month-old knock-in rats (Fig. 1a and 1b). Finally, AT8 antibody showed no staining in any of the animals studied (Fig. 1a and 1b).

Gene-dosage-dependent amyloid pathology in App^{s}: $Psen1^{LF}$ **mutant knock-in rats.** *Psen1 L435F* homozygote mutant mice are perinatally lethal [16] in a manner that resembles the early embryonic lethality of *Psen1* knockout mice [31]. This is likely the result of the PS1 L435F-mediated disruption of Notch signaling. Unexpectedly, we found that homozygote $App^{h/h}$:$Psen1^{LF/LF}$ rats are born in Mendelian ratios, survive into adulthood, and have preserved neurodevelopment and Notch signaling, despite altered APP metabolism [26]. Based on this evidence, we reexamined whether interactions of these two pathogenic mutations cause amyloid pathology, focusing our attention on genotypes carrying two mutant $Psen1^{LF}$ alleles ($App^{h/h}$:$Psen1^{LF/LF}$, $App^{s/h}$:$Psen1^{LF/LF}$, and $App^{s/s}$:$Psen1^{LF/LF}$) in addition to $App^{h/h}$:$Psen1^{w/w}$ control animals and $App^{h/h}$:$Psen1^{LF/w}$ rats that were not tested at 18 months of age. Given that homozygous $Psen1^{LF}$ mutant rats show increased postnatal lethality [26], animals were tested

at 14 months of age. We analyzed the following rat subjects: $App^{h/h}$:$Psen1^{w/w}$, 7 males and 7 females; $App^{h/h}$:$Psen1^{LF/LF}$, 2 males and 4 females; $App^{s/h}$:$Psen1^{LF/LF}$, 6 males and 6 females; $App^{s/s}$:$Psen1^{LF/LF}$, 8 males and 2 females; $App^{h/h}$:$Psen1^{LF/w}$, 2 males and 3 females.

Representative images of H&E staining of dorsal hippocampus and sensory cortex (Fig. 2a) and of magnified area of the CA1 illustrate very similar structures within these brain regions for all knock-in rats (Fig. 2b). A comparison of the male and female cohorts did not show evidence of a gender driven difference. One $App^{h/h}$:$Psen1^{LF/LF}$ sample, subject 437 (S437), presented hydrocephalus and $App^{h/h}$:$Psen1^{LF/w}$ S439 had a large tumor compressing the hypothalamus. Otherwise, all the subjects showed no evidence of gross structural changes in comparison to the control $App^{h/h}$:$Psen1^{w/w}$ subjects. No apparent neurodegeneration-related defects were evident in these animals and there was no evidence of pyknotic stressed or dying neurons.

No overt neuronal loss was observed in the NeuN-stained sections. A representative subject from each of the groups studied is illustrated in Fig. 2a. Magnified area of the CA1 also illustrate very similar structures within the hippocampus for all knock-in groups (Fig. 2b). Blinded qualitative analysis confirmed there was no obvious difference in NeuN density among the nine groups (see **Table 1**). However, $App^{s/h}$:$Psen1^{LF/LF}$ S414 and $App^{s/s}$:$Psen1^{LF/LF}$ S426 presented focal neurodegeneration with pyknotic cells, in the CA1 layer of the dorsal hippocampus (Fig. 3).

No dense clusters of astrocytes were apparent with GFAP staining in the majority of 14-month-old knock-in rat, and an even distribution of GFAP expression was observed throughout the brain. A representative subject from each genotype is illustrated in Fig. 2a. A magnified area of the CA1 also illustrates very similar astrocytic activation within the hippocampus for the FAD mutant knock-in rats groups compared to the control animals (Fig. 2b). Overall, there is no evidence of a widespread astrocytic inflammatory response related to the genotype. The only exceptions where clear astrocytic activation surrounding the CA1 focal degeneration in $App^{s/h}$:$Psen1^{LF/LF}$ S414 and $App^{s/s}$:$Psen1^{LF/LF}$ S426 (Fig. 3), three animals with widespread activation, $App^{w/w}$:$Psen1^{LF/w}$ S438/S439 and $App^{s/s}$:$Psen1^{LF/LF}$ S418 (suspected to be related to the presence of a pituitary tumor, not shown). Microglial foci and areas found with activated microglia (see below) did not appear to be associated with astrocytic activation. Both the female and male cohorts have very similar GFAP staining patterns. Blinded qualitative analysis confirmed there was no obvious difference in astrocytic activation within the knock-in and WT groups (**Table 2**).

Overall, Iba1 staining did not reveal clear evidence of microglial inflammatory response related to the genotype, i.e., a feature consistent in most of the samples of the group. A representative subject from each of the 14-month-old knock-in FAD and control groups is illustrated in Fig. 2a. A magnified area of the CA1 illustrate similar activation levels within the hippocampus for the FAD knock-in rats compared to the control knock-in animals (Fig. 2b). Throughout the brain, the morphology of the microglia is generally ramified, without patches of bushy activated microglia or inflammatory foci and both female and male cohorts have very similar Iba1 staining patterns. Blinded qualitative analysis indicated that, overall, there

was no obvious difference in microglial activation within the FAD and control knock-in groups (**Table 2)**. However, there were some brain areas with localized microglia activation in few subjects (summarized in **Table 3**). In the two subjects with CA1 focal degeneration (*App*$^{s/h}$:*Psen1*$^{LF/LF}$ S414, and *App*$^{s/s}$:*Psen1*$^{LF/LF}$ S426), microglia were highly activated in very close proximity to the degenerating CA1 (Fig. 3). Areas with microglial activation (defined as activated microglia spread apart in an area/part of a brain structure, Fig. 4) and microglial foci (defined as an area with activated microglia regrouped and seemingly attracted toward a focal point, Fig. 5) were observed in 1 *App*$^{h/h}$:*Psen1*$^{LF/w}$ (S441), 1 *App*$^{h/h}$:*Psen1*$^{LF/LF}$ (S432), 4 *App*$^{s/h}$:*Psen1*$^{LF/LF}$ (S421, S412, S446, S438) and 4 *App*$^{s/s}$:*Psen1*$^{LF/LF}$ (S419, S420, S444, S426) subjects, but not in *App*$^{h/h}$:*Psen1*$^{w/w}$ control samples. These areas were located in various brain structures, including thalamus, white matter, amygdala, CA1/CA2, entorhinal cortex, frontal cortex and striatum.

A 6E10 and 4G8 antibody mix was used to investigate the presence of amyloid plaques. A representative subject from each group is illustrated in Fig. 2a. All 10 *App*$^{s/s}$:*Psen1*$^{LF/LF}$ animals presented amyloid plaques. The plaque morphology was usually round, small, dense, and they were present in small clusters. Plaques were slightly more numerous, larger, and more frequently located in the cortex (in 100% of *App*$^{s/s}$:*Psen1*$^{LF/LF}$), and randomly distributed across the cortical mantle; no particular sub-region was more affected. A few small plaques were located in the hippocampus (in 80% of *App*$^{s/s}$:*Psen1*$^{LF/LF}$), more specifically between the dentate gyrus and CA1. Some plaques were also found in the corpus callosum (in 50% of *App*$^{s/s}$:*Psen1*$^{LF/LF}$), and finally, one plaque in the thalamus (in 20% of *App*$^{s/s}$:*Psen1*$^{LF/LF}$) (Fig. 6). In addition, strong to moderate amyloid deposition was also observed in the leptomeningeal blood vessels walls in 5 out of 10 *App*$^{s/s}$:*Psen1*$^{LF/LF}$ animals (see Fig. 6 and summary **Table 2**). Moderate to low deposition in the cortex vasculature of the brain was also observed in animals with leptomeningeal deposition (see Fig. 6). In the *App*$^{s/h}$:*Psen1*$^{LF/LF}$ group, 2 out of 12 animals had 2–3, very small amyloid plaques (S456, S415) and two animals had deposits in the leptomeningeal vessels (S414, S455). No 6E10/4G8 staining was observed in any animals from the other genotypes. No staining with AT8 was observed in any of the animals studied, consistent with the absence of silver staining positive tangles. A representative animal from each group is illustrated in Fig. 2a. The modified Bielshowski Silver stain was used to identify plaque structures in the tissue, along with aberrant neuronal inclusion such as tangles, and apoptotic driven cell death. A representative subject from each of the groups is illustrated in Fig. 2a. A magnified area of the CA1 illustrate very similar structures within the hippocampus for the knock-in rats groups compared to the wild type animals (Fig. 2b).

Amyloid plaques of App$^{s/s}$:Psen1$^{LF/LF}$ **and** App$^{s/h}$:Psen1$^{LF/LF}$ **knock-in rats are composed of Aβ40, Aβ42 and Aβ43.** Composition of the Amyloid plaques was evaluated with antibodies directed against Aβ40, Aβ42, Aβ43 and the 6E10/4G8 mix (pan-Aβ). Antibodies directed against Aβ40, Aβ42, Aβ43 allow to identify the Aβ species forming amyloid plaques and, unlike 6E10 and 4G8, do not bind APP, APP-CTFs and large sAPP molecules. Consecutive slices were stained in the following order Aβ42 > Aβ40 > Aβ43 > pan-Aβ (Fig. 7a). The samples stained were: 4 *App*$^{h/h}$:*Psen1*$^{w/w}$ control animals, the 2 *App*$^{s/h}$:*Psen1*$^{LF/LF}$ animals with a few plaques (S456, S415) and all the *App*$^{s/s}$:*Psen1*$^{LF/LF}$ animals. Plaques appeared

positive for all the Aβ isoforms studied in all the animals studied, i.e. when a plaque was spanning across the 4 slides it was positive for Aβ40, Aβ42 and Aβ43. Location of the plaques did not appear to affect its composition, i.e. all the Aβ isoforms were present in plaques located in the cortex, hippocampus or corpus callosum. It appeared that Aβ40 and Aβ42 were mainly present in the center of the plaques whereas Aβ43 was present in the center and border of the plaques (Fig. 7b). No Aβ40, Aβ42, Aβ43 or pan-Aβ was observed in the $App^{h/h}$:$Psen1^{w/w}$ control animals. The very small plaques from the 2 $App^{s/h}$:$Psen1^{LF/LF}$ S456 and S415, were also positive for all the Aβ isoforms tested.

To assess the presence of activated astrocytes and microglia in the vicinity of amyloid plaques we analyzed consecutive 6E10/4G8, GFAP and Iba1 stained slides. A few mildly activated astrocytes and microglia were found surrounding the largest plaques, their low number and moderately activated morphology suggested relatively young plaque formation (see Fig. 7c). Therefore, plaque-induced microglial activation was present but limited.

Silver stained plaque formations were not as abundant as the amyloid staining, and were not as frequently observed in $App^{s/s}$:$Psen1^{LF/LF}$ tissues. When present, the silver staining of amyloid plaques appeared light and not as dark as mature plaques are usually observed in the literature. Only the largest, rare, round plaques in the cortex could be observed, clusters of small plaques were not visible with silver staining. Plaque locations were more apparent due to darker circular staining circumscribing the periphery of the plaque rather than the plaque themselves (see Fig. 7d). Together, these observations suggest relatively young plaques, which is consistent with the small plaque size and the mild microglia and GFAP activation surrounding them. We did not observe neurons bearing tau tangles in the surroundings of the plaques nor anywhere else in the brain.

Knock-in rats that develop amyloid pathology have highest CNS Aβ43 levels. The evidence that 14 months old $App^{s/s}$:$Psen1^{LF/LF}$ have a low number of young plaques and that only ~ 16% of $App^{s/h}$:$Psen1^{LF/LF}$ animals showed 2–3 small plaques, indicates recent amyloid deposition in these rats. Thus, to measure CNS Aβ species composition needed to initiate amyloid deposition we performed Aβ ELISA measurements in 7 month-old rats. To produce rats carrying all possible genetic permutations of these two mutants, we crossed male and female $App^{s/h}$:$Psen1^{LF/w}$ rats. Animals of all 9 possible genetic combinations were obtained: $App^{h/h}$:$Psen1^{w/w}$, $App^{s/h}$:$Psen1^{w/w}$, $App^{s/s}$:$Psen1^{w/w}$, $App^{h/h}$:$Psen1^{LF/w}$, $App^{s/h}$:$Psen1^{LF/w}$, $App^{s/s}$:$Psen1^{LF/w}$, $App^{h/h}$:$Psen1^{LF/LF}$, $App^{s/h}$:$Psen1^{LF/LF}$, and $App^{s/s}$:$Psen1^{LF/LF}$.

First, we determined if and how the interaction of these two pathogenic mutations alter Aβ species profiles. Brains were harvested from ~ 7 months old rats and levels of Aβ38, Aβ40, Aβ42 and Aβ43 were measured by ELISA. These four Aβ species are the products of the 3rd and 4th catalytic steps of product line 1 (Aβ43 and Aβ40) and product line 2 (Aβ42 and Aβ38). All data relating to these experiments are shown in Fig. 8a. The detailed statistical analyses are shown in Fig. 8b. Aβ38 was barely detectable in control animals, undetectable in $App^{h/h}$:$Psen1^{LF/w}$ and $App^{h/h}$:$Psen1^{LF/LF}$ rats, and augmented in Swedish rats in a gene-dosage dependent manner. The Swedish mutation-dependent increase in Aβ38 was

significantly reduced by one *Psen1*^{LF} allele and was occluded by two *Psen1*^{LF} alleles. A similar pattern was observed for Aβ40, which was increased and decreased in a gene-dosage-dependent manner by the *App*^{s} and *Psen1*^{LF} mutations, respectively. The *Psen1*^{LF} allele significantly reduced, in a gene-dosage-dependent manner, the increase in Aβ40 caused by the Swedish mutation. Aβ42 levels were increased by the Swedish mutation in a gene-dosage-dependent manner, but were not significantly altered by the *Psen1*^{LF} mutation. Yet, the *Psen1*^{LF} mutation further boosted the increase in Aβ42 levels caused by *App*^{s}. A gene-dosage-dependent increase in Aβ43 levels was observed in rats carrying the *Psen1*^{LF} mutation. Aβ43 levels were higher than control in both heterozygous and homozygous *App*^{s} rat, but the increase was not statistically significant in this two-way ANOVA analysis. One-way ANOVA analysis of *App*$^{h/h}$:*Psen1*$^{w/w}$, *App*$^{s/h}$:*Psen1*$^{w/w}$ and *App*$^{s/s}$:*Psen1*$^{w/w}$ samples showed a gene-dosage dependent increase in Aβ43 in *App*^{s} rats, when in combination with one or both *Psen1*^{LF} alleles; however, given the large effect size of the *Psen1*^{LF} allele on Aβ43 production, when you analyze the *Psen1*^{w}-only animals separately, a statistically significant increase in Aβ43 caused by the *App*^{s} allele is evident as well(Fig. 8c). In line with these observations, we found a synergistic effect of the two pathogenic mutations on Aβ43 levels, with exceptionally high levels of Aβ43 in *App*$^{s/h}$:*Psen1*$^{LF/LF}$ and, yet more, in *App*$^{s/s}$:*Psen1*$^{LF/LF}$ rats.

As discussed above, increase in the Aβ42/Aβ40 ratio is considered a predictor of amyloid pathology and AD. This ratio was increased by the *Psen1*^{LF} mutation in a gene-dosage dependent manner but was unaffected by the Swedish mutation. Moreover, the Swedish mutation reduced the increase of these ratios caused by the *Psen1*^{LF} mutation in a gene-dosage dependent manner. We extended this analysis to the Aβ43/Aβ40 and Aβ43/Aβ42 ratios and observed identical patterns. All data relative to these experiments are shown in Fig. 9a, with the detailed statistical analyses shown in Fig. 9b.

To quantify γ-secretase processivity, Chávez-Gutiérrez's lab has introduced a ratio between the sum of the products of the 4th catalytic turnover divided by the sum of the products of the 3rd catalytic step, which are the substrates of the 4th catalytic turnover [9]. Ultimately, this ratio provides an overall measure of γ-secretase processivity along both product lines. Applying this method to an *in vitro* analysis of Aβ profiles of 25 FAD-linked PSEN1 mutants, the authors found a linear correlation between mutation-driven alterations in Aβ profiles and age at onset of AD in humans [9]. Hence, to assess γ-secretase processivity in our 9 rat lines we calculated the Aβ (38 + 40)/(42 + 43) ratios. We observed a gene-dosage-dependent reduction of γ-secretase processivity caused by the *Psen1*^{LF} mutation; in contrast, the Swedish mutation did not significantly change γ-secretase processivity, regardless of the *Psen1* genotype (Fig. 9a and 9b).

Overall, the data indicate that co-expression of the *Psen1*^{LF} and the Swedish mutations cause both synergistic and opposite effects on Aβ brain composition in a gene-dosage-dependent manner: Aβ43 production is synergistically increased by the two FAD mutation, while the *Psen1*^{LF} mutation obliterates Aβ38 production, which is increased by the Swedish mutation.

Discussion

Understanding the changes in molecular composition of Aβ profiles that are needed to initiate amyloid deposition is a central question in the context of the amyloid hypothesis of AD pathogenesis. To provide insights into the composition of pathogenic Aβ cocktails we have studied knock-in rats expressing 8 permutations of the FAD *APP* Swedish and *PSEN1 L435F* mutations. The APP mutation's primary effect is to increase the levels of the γ-secretase substrate and Aβ precursor APP-βCTF. This leads to a gene-dosage -dependent increase in all Aβ species analyzed (i.e., Aβ38. Aβ40, Aβ42 and Aβ43). In contrast, the *PSEN1 L435F* decreases the activity and processivity of γ-secretase. As a result, this mutation causes a gene-dosage-dependent shift from shorter to longer Aβ species leading to a decrease in total Aβ amounts. This shift is dramatically obvious for the Aβ product line 1, as shown by the large increase in Aβ43, generated by the 3rd catalytic step, concurrent with a large decrease in Aβ40, which is derived from Aβ43 in the 4th catalytic step. Coexistence of the two mutations in the same subject causes both synergistic and opposite effects on Aβ brain composition. For example, the two pathogenic mutations synergistically increase Aβ43 levels in a gene-dosage-dependent manner. In contrast, the $Psen1^{LF}$ allele significantly reduces, also in a gene-dosage-dependent manner, the increase in Aβ40 and Aβ38 caused by the Swedish mutation. These changes can be rationally explained by expression of γ-secretase with reduced activity/processivity concurrent with increased availability of APP-βCTF.

IHC analysis shows that, at 14 months of age, 100% (10 out of 10) of $App^{s/s}$:$Psen1^{LF/LF}$ rats develop amyloid pathology. Plaques are seen in several brain regions, including the cortical mantle, hippocampus, corpus callosum and thalamus. In 50% of the animals, amyloid deposition is also observed in the leptomeningeal blood vessels walls. Plaques are composed by Aβ40, Aβ42 and Aβ43, with Aβ40 and Aβ42 mainly present in the center of the plaques and Aβ43 present in the center and border of the plaques. Plaques are mostly round, small and dense, with few larger plaques that are mainly located in the cortex. In silver staining, amyloid plaques appear light, which contrasts the dark aspect of mature plaques. A few mildly activated microglia surround the largest plaques. Altogether, these observations suggest relatively young plaque formation. Two out of 12 $App^{s/h}$:$Psen1^{LF/LF}$ animals (16.6%) had 2–3, very small amyloid plaques and two animals had deposits in the leptomeningeal vessels. No amyloid plaques are detected in the other genotypes analyzed at either 14 ($App^{h/h}$:$Psen1^{LF/w}$, $App^{h/h}$:$Psen1^{LF/LF}$) or 18 ($App^{s/h}$:$Psen1^{w/w}$, $App^{s/s}$:$Psen1^{w/w}$, $App^{s/h}$:$Psen1^{LF/w}$ and $App^{s/s}$:$Psen1^{LF/w}$) months of age. In summary, development of amyloid pathology requires co-expression of two $Psen1^{LF}$ mutant alleles with at least one App^{s} mutant allele: doubling the App^{s} load significantly accelerated amyloid deposition.

The evidence that 14 months old $App^{s/s}$:$Psen1^{LF/LF}$ have a low number of relatively young plaques and that only ~ 16% of $App^{s/h}$:$Psen1^{LF/LF}$ animals showed 2–3 small plaques, indicates that the ELISA measurements performed in 7 month-old rats reflect pre-pathological CNS Aβ species composition needed to initiate amyloid deposition. Comparing the genetic make-up leading to amyloid pathology with the quantification of Aβ species leads to the following conclusions. 1) Aβ42/Aβ40, Aβ43/Aβ40 and Aβ43/Aβ42 ratios values follow this hierarchy: $App^{h/h}$:$Psen1^{LF/LF}$ > $App^{s/h}$:$Psen1^{LF/LF}$ > $App^{s/s}$:$Psen1^{LF/LF}$. Yet, $App^{h/h}$:$Psen1^{LF/LF}$ show no plaques, $App^{s/h}$:$Psen1^{LF/LF}$ show few plaques in 16% of the subjects, while $App^{s/s}$:$Psen1^{LF/LF}$ show more plaques in 100% of the subjects analyzed. Thus, amyloid plaques

deposition is not associated with highest long-Aβ/short-Aβ ratios. In fact, 2) Aβ42 levels are significantly higher in *App*$^{s/s}$:*Psen1*$^{LF/w}$ as compared to *App*$^{s/h}$:*Psen1*$^{LF/LF}$ animals (P < 0.0001). Yet, *App*$^{s/h}$:*Psen1*$^{LF/LF}$ rats start showing signs of plaques deposition at 14 months of age while *App*$^{s/s}$:*Psen1*$^{LF/w}$ animals to do not show any amyloid plaques even at 18 months of age. 3) Amyloid plaques are detected in the genotypes with highest levels of Aβ43 (*App*$^{s/s}$:*Psen1*$^{LF/LF}$ and *App*$^{s/h}$:*Psen1*$^{LF/LF}$ animals), in a manner proportional to Aβ43 levels (Aβ43 levels: *App*$^{s/s}$:*Psen1*$^{LF/LF}$ > *App*$^{s/h}$:*Psen1*$^{LF/LF}$, P < 0.0001). Although a complete analysis of all Aβ species generated along products line 1 (Aβ49 → Aβ46 → Aβ43 → Aβ40 → Aβ37, which is a minor product of a 5th catalytic step) and 2 (Aβ48 → Aβ45 → Aβ42 → Aβ38) would make this analysis exhaustive, the data reported here indicate that the CNS levels of Aβ43, rather than Aβ species' ratios and absolute levels of Aβ42, determine the speed of pathological amyloid deposition.

Several studies have shown that FAD mutations cause a significant increase in Aβ43 levels. These studies include analysis of PSEN1-R278I in *Presenilins* knock-out mouse embryonal fibroblast (MEFs) [34], PSEN1-R278I, -C410Y and -L435H in HEK cells and MEFs [35–37], PSEN1-V261F, -R278I, -L435F, -L166P, -Y256S, G382A in HEK293/swe cells [38], PSEN1-R278I [34], PSEN1-I213T [39] and PSEN1-P117L [40] in knock-in mice, PSEN1-L435F patient-derived iPSC-neurons [41]. Moreover, Aβ43 has also been found in amyloid plaque lesions of 7 cases with the APP Swedish mutation and 3 cases with the PSEN1-I143T FAD mutation [42–44], as well as two cases with the PSEN1-L435F mutation [37]. Most importantly, Aβ43 has also been described in late onset sporadic AD cases [37, 42, 44], and CSF level of Aβ43 is a significant predictor of mild cognitive impairment (MCI) and cerebral amyloid deposits [33]. Also, a 2-year follow up study showed that CSF levels of Aβ43, not Aβ42, decreased in patients who progressed from MCI patients to sporadic AD [45], suggesting a faster rate of Aβ43 deposition as compared to Aβ42 deposition. Interestingly, the mean age of onset in patients carrying the Swedish mutation is 55 years with a range of 45–61 years, and the mean duration of the illness is 7 years [46]. In contrast, the average age of onset in patients carrying the *PSEN1-L435F* mutation is 47 years, and the average age at death is 56 years [29]. The higher aggressiveness of the *PSEN1-L435F* mutation associates with the significantly higher levels of Aβ43 production detected in *Psen1*^{LF} rats compared to *App*^{s} rats. Altogether, the above data support the hypothesis that Aβ43 could play a major role in determining the onset of pathological amyloid deposition in both familial and sporadic AD.

In conclusion, this study corroborates the critical pathological importance of alterations in the Aβ peptides composition, helps clarifying the molecular determinants initiating amyloid pathology, and supports therapeutic interventions targeting Aβ43 to prevent, delay, or revert AD.

Declarations

Ethics approval and consent to participate: Ethical care and use of animals in accordance with the Ethical Guidelines for Treatment of Laboratory Animals of the NIH. The procedures were described and approved by the Institutional Animal Care and Use Committee (IACUC) at Rutgers (PROTO201702513).

Consent for publication: Not applicable.

Availability of data and materials: The datasets and materials used and/or analyzed during the current study are available from the corresponding author on reasonable request.

Competing interests: The authors declare that they have no competing interests.

Funding: National Institute on Aging (To LD: R01AG073182, R01 AG063407, and RF1 AG064821; to M.D.T: K99AG065441)

Authors' contributions: M.D.T., T.Y. and L.D. designed the experiments and analyzed the results. L.D. designed the KI rats. M.D.T., T.Y., L.B. and S. Z. performed the experiments. L.D. wrote the manuscript. M.D.T., T.Y. and M.Y. edited the manuscript.

Acknowledgements: All authors read and approved the final manuscript.

Dedication: We want to dedicate this manuscript to the memory of Huaxi Xu.

Authors' information: Department of Pharmacology, Physiology & Neuroscience New Jersey Medical School, Brain Health Institute, Jacqueline Krieger Klein Center in Alzheimer's Disease and Neurodegeneration Research, Rutgers, The State University of New Jersey, 205 South Orange Ave, Newark, NJ, 07103, USA. M.D.T., T.Y., M.Y. and L.D.

Biospective Inc., Montreal, Quebec, Canada. L.B. and S.Z.

References

1. S. F. Lichtenthaler, C. Haass, and H. Steiner, "Regulated intramembrane proteolysis–lessons from amyloid precursor protein processing," (in eng), *J Neurochem*, vol. 117, no. 5, pp. 779 – 96, Jun 2011, doi: 10.1111/j.1471-4159.2011.07248.x.

2. C. Haass and D. J. Selkoe, "Soluble protein oligomers in neurodegeneration: lessons from the Alzheimer's amyloid beta-peptide," (in eng), *Nat Rev Mol Cell Biol*, vol. 8, no. 2, pp. 101 – 12, Feb 2007, doi: 10.1038/nrm2101.

3. M. Citron *et al.*, "Mutation of the beta-amyloid precursor protein in familial Alzheimer's disease increases beta-protein production," *Nature*, vol. 360, no. 6405, pp. 672-4, Dec 17 1992, doi: 10.1038/360672a0.

4. T. Saito *et al.*, "Single App knock-in mouse models of Alzheimer's disease," (in eng), *Nat Neurosci*, vol. 17, no. 5, pp. 661-3, May 2014, doi: 10.1038/nn.3697.

5. M. D. Tambini, W. Yao, and L. D'Adamio, "Facilitation of glutamate, but not GABA, release in Familial Alzheimer's APP mutant Knock-in rats with increased beta-cleavage of APP," *Aging Cell*, vol. 18, no. 6, p. e13033, Dec 2019, doi: 10.1111/acel.13033.

6. T. Jonsson *et al.*, "A mutation in APP protects against Alzheimer's disease and age-related cognitive decline," (in eng), *Nature*, vol. 488, no. 7409, pp. 96 – 9, Aug 02 2012, doi: 10.1038/nature11283.

7. M. D. Tambini, K. A. Norris, and L. D'Adamio, "Opposite changes in APP processing and human Aβ levels in rats carrying either a protective or a pathogenic APP mutation," (in eng), *Elife*, vol. 9, 02 2020, doi: 10.7554/eLife.52612.

8. M. Szaruga *et al.*, "Alzheimer's-Causing Mutations Shift Aβ Length by Destabilizing γ-Secretase-Aβn Interactions," (in eng), *Cell*, vol. 170, no. 3, pp. 443–456.e14, Jul 27 2017, doi: 10.1016/j.cell.2017.07.004.

9. D. Petit *et al.*, "Aβ profiles generated by Alzheimer's disease causing PSEN1 variants determine the pathogenicity of the mutation and predict age at disease onset," (in eng), *Mol Psychiatry*, vol. 27, no. 6, pp. 2821–2832, Jun 2022, doi: 10.1038/s41380-022-01518-6.

10. D. Scheuner *et al.*, "Secreted amyloid beta-protein similar to that in the senile plaques of Alzheimer's disease is increased in vivo by the presenilin 1 and 2 and APP mutations linked to familial Alzheimer's disease," (in eng), *Nat Med*, vol. 2, no. 8, pp. 864 – 70, Aug 1996, doi: 10.1038/nm0896-864.

11. D. R. Borchelt *et al.*, "Familial Alzheimer's disease-linked presenilin 1 variants elevate Abeta1-42/1–40 ratio in vitro and in vivo," (in eng), *Neuron*, vol. 17, no. 5, pp. 1005-13, Nov 1996, doi: S0896-6273(00)80230-5 [pii].

12. K. Duff *et al.*, "Increased amyloid-beta42(43) in brains of mice expressing mutant presenilin 1," (in eng), *Nature*, vol. 383, no. 6602, pp. 710-3, Oct 24 1996, doi: 10.1038/383710a0.

13. M. Citron *et al.*, "Mutant presenilins of Alzheimer's disease increase production of 42-residue amyloid beta-protein in both transfected cells and transgenic mice," (in eng), *Nat Med*, vol. 3, no. 1, pp. 67–72, Jan 1997, doi: 10.1038/nm0197-67.

14. O. Murayama *et al.*, "Enhancement of amyloid beta 42 secretion by 28 different presenilin 1 mutations of familial Alzheimer's disease," (in eng), *Neurosci Lett*, vol. 265, no. 1, pp. 61 – 3, Apr 09 1999, doi: 10.1016/s0304-3940(99)00187-1.

15. T. Tomita *et al.*, "The presenilin 2 mutation (N141I) linked to familial Alzheimer disease (Volga German families) increases the secretion of amyloid beta protein ending at the 42nd (or 43rd) residue," (in eng), *Proc Natl Acad Sci U S A*, vol. 94, no. 5, pp. 2025-30, Mar 04 1997, doi: 10.1073/pnas.94.5.2025.

16. D. Xia *et al.*, "Presenilin-1 Knockin Mice Reveal Loss-of-Function Mechanism for Familial Alzheimer's Disease," (in eng), *Neuron*, vol. 85, no. 5, pp. 967 – 81, Mar 4 2015, doi: 10.1016/j.neuron.2015.02.010.

17. S. Kumar-Singh *et al.*, "Mean age-of-onset of familial alzheimer disease caused by presenilin mutations correlates with both increased Abeta42 and decreased Abeta40," (in eng), *Hum Mutat*, vol. 27, no. 7, pp. 686 – 95, Jul 2006, doi: 10.1002/humu.20336.

18. S. Hsu *et al.*, "Systematic validation of variants of unknown significance in APP, PSEN1 and PSEN2," (in eng), *Neurobiol Dis*, vol. 139, p. 104817, 06 2020, doi: 10.1016/j.nbd.2020.104817.

19. M. Duering, M. O. Grimm, H. S. Grimm, J. Schröder, and T. Hartmann, "Mean age of onset in familial Alzheimer's disease is determined by amyloid beta 42," (in eng), *Neurobiol Aging*, vol. 26, no. 6, pp. 785-8, Jun 2005, doi: 10.1016/j.neurobiolaging.2004.08.002.

20. N. D. Mehta *et al.*, "Increased Abeta42(43) from cell lines expressing presenilin 1 mutations," (in eng), *Ann Neurol*, vol. 43, no. 2, pp. 256-8, Feb 1998, doi: 10.1002/ana.410430217.

21. L. Sun, R. Zhou, G. Yang, and Y. Shi, "Analysis of 138 pathogenic mutations in presenilin-1 on the in vitro production of Abeta42 and Abeta40 peptides by gamma-secretase," *Proc Natl Acad Sci U S A*, vol. 114, no. 4, pp. E476-E485, Jan 24 2017, doi: 10.1073/pnas.1618657114.

22. M. A. Fernandez, J. A. Klutkowski, T. Freret, and M. S. Wolfe, "Alzheimer presenilin-1 mutations dramatically reduce trimming of long amyloid β-peptides (Aβ) by γ-secretase to increase 42-to-40-residue Aβ," (in eng), *J Biol Chem*, vol. 289, no. 45, pp. 31043-52, Nov 07 2014, doi: 10.1074/jbc.M114.581165.

23. S. Veugelen, T. Saito, T. C. Saido, L. Chavez-Gutierrez, and B. De Strooper, "Familial Alzheimer's Disease Mutations in Presenilin Generate Amyloidogenic Abeta Peptide Seeds," *Neuron*, vol. 90, no. 2, pp. 410-6, Apr 20 2016, doi: 10.1016/j.neuron.2016.03.010.

24. B. Kretner *et al.*, "Generation and deposition of Abeta43 by the virtually inactive presenilin-1 L435F mutant contradicts the presenilin loss-of-function hypothesis of Alzheimer's disease," *EMBO Mol Med*, vol. 8, no. 5, pp. 458 – 65, May 2016, doi: 10.15252/emmm.201505952.

25. L. Chávez-Gutiérrez *et al.*, "The mechanism of γ-Secretase dysfunction in familial Alzheimer disease," (in eng), *EMBO J*, vol. 31, no. 10, pp. 2261-74, May 16 2012, doi: 10.1038/emboj.2012.79.

26. M. D. Tambini and L. D'Adamio, "Knock-in rats with homozygous *PSEN1* ^{L435F} Alzheimer mutation are viable and show selective γ-secretase activity loss causing low Aβ40/42 and high Aβ43," (in eng), *J Biol Chem*, vol. 295, no. 21, pp. 7442–7451, May 2020, doi: 10.1074/jbc.RA120.012542.

27. J. A. Johnston *et al.*, "Increased beta-amyloid release and levels of amyloid precursor protein (APP) in fibroblast cell lines from family members with the Swedish Alzheimer's disease APP670/671 mutation," *FEBS Lett*, vol. 354, no. 3, pp. 274-8, Nov 14 1994.

28. M. Citron *et al.*, "Excessive production of amyloid beta-protein by peripheral cells of symptomatic and presymptomatic patients carrying the Swedish familial Alzheimer disease mutation," *Proc Natl Acad Sci U S A*, vol. 91, no. 25, pp. 11993-7, Dec 6 1994.

29. E. A. Heilig, W. Xia, J. Shen, and R. J. Kelleher, 3rd, "A presenilin-1 mutation identified in familial Alzheimer disease with cotton wool plaques causes a nearly complete loss of gamma-secretase activity,"

(in eng), *J Biol Chem*, Research Support, N.I.H., Extramural Research Support, Non-U.S. Gov't vol. 285, no. 29, pp. 22350-9, Jul 16 2010, doi: 10.1074/jbc.M110.116962.

30. M. Szaruga *et al.*, "Alzheimer's-causing mutations shift Aβ length by destabilizing γ-secretase-Aβn interactions," (in eng), *Cell*, vol. 184, no. 8, pp. 2257–2258, Apr 15 2021, doi: 10.1016/j.cell.2021.03.058.

31. J. Shen, R. T. Bronson, D. F. Chen, W. Xia, D. J. Selkoe, and S. Tonegawa, "Skeletal and CNS defects in Presenilin-1-deficient mice," (in eng), *Cell*, vol. 89, no. 4, pp. 629 – 39, May 16 1997, doi: S0092-8674(00)80244-5 [pii].

32. N. Tolboom *et al.*, "Relationship of cerebrospinal fluid markers to 11C-PiB and 18F-FDDNP binding," (in eng), *J Nucl Med*, vol. 50, no. 9, pp. 1464-70, Sep 2009, doi: 10.2967/jnumed.109.064360.

33. I. S. Almdahl *et al.*, "Cerebrospinal Fluid Levels of Amyloid Beta 1–43 Mirror 1–42 in Relation to Imaging Biomarkers of Alzheimer's Disease," (in eng), *Front Aging Neurosci*, vol. 9, p. 9, 2017, doi: 10.3389/fnagi.2017.00009.

34. T. Saito *et al.*, "Potent amyloidogenicity and pathogenicity of Aβ43," *Nature Neuroscience*, vol. 14, no. 8, pp. 1023–1032, 2011/08/01 2011, doi: 10.1038/nn.2858.

35. Y. Nakaya *et al.*, "Random Mutagenesis of Presenilin-1 Identifies Novel Mutants Exclusively Generating Long Amyloid β-Peptides *," *Journal of Biological Chemistry*, vol. 280, no. 19, pp. 19070–19077, 2005, doi: 10.1074/jbc.M501130200.

36. S. Veugelen, T. Saito, Takaomi C. Saido, L. Chávez-Gutiérrez, and B. De Strooper, "Familial Alzheimer's Disease Mutations in Presenilin Generate Amyloidogenic Aβ Peptide Seeds," *Neuron*, vol. 90, no. 2, pp. 410–416, 2016, doi: 10.1016/j.neuron.2016.03.010.

37. B. Kretner *et al.*, "Generation and deposition of Aβ43 by the virtually inactive presenilin-1 L435F mutant contradicts the presenilin loss-of-function hypothesis of Alzheimer's disease," (in eng), *EMBO Mol Med*, vol. 8, no. 5, pp. 458 – 65, 05 2016, doi: 10.15252/emmm.201505952.

38. J. Trambauer, R. M. Rodríguez Sarmiento, A. Fukumori, R. Feederle, K. Baumann, and H. Steiner, "Aβ43-producing PS1 FAD mutants cause altered substrate interactions and respond to γ-secretase modulation," *EMBO reports*, https://doi.org/10.15252/embr.201947996 vol. 21, no. 1, p. e47996, 2020/01/07 2020, doi: https://doi.org/10.15252/embr.201947996.

39. M. Shimojo *et al.*, "Enzymatic Characteristics of I213T Mutant Presenilin-1/γ-Secretase in Cell Models and Knock-in Mouse Brains: FAMILIAL ALZHEIMER DISEASE-LINKED MUTATION IMPAIRS γ-SITE CLEAVAGE OF AMYLOID PRECURSOR PROTEIN C-TERMINAL FRAGMENT β *," *Journal of Biological Chemistry*, vol. 283, no. 24, pp. 16488–16496, 2008, doi: 10.1074/jbc.M801279200.

40. K. Sato *et al.*, "A third-generation mouse model of Alzheimer's disease shows early and increased cored plaque pathology composed of wild-type human amyloid β peptide," *Journal of Biological Chemistry*, vol. 297, no. 3, 2021, doi: 10.1016/j.jbc.2021.101004.

41. D. H. Oakley, M. Chung, N. Klickstein, C. Commins, B. T. Hyman, and M. P. Frosch, "The Alzheimer Disease-Causing Presenilin-1 L435F Mutation Causes Increased Production of Soluble Aβ43 Species in Patient-Derived iPSC-Neurons, Closely Mimicking Matched Patient Brain Tissue," *Journal of Neuropathology & Experimental Neurology*, vol. 79, no. 6, pp. 592–604, 2020, doi: 10.1093/jnen/nlaa025.

42. H. Welander, J. Frånberg, C. Graff, E. Sundström, B. Winblad, and L. O. Tjernberg, "Aβ43 is more frequent than Aβ40 in amyloid plaque cores from Alzheimer disease brains," *Journal of Neurochemistry*, vol. 110, no. 2, pp. 697–706, 2009, doi: https://doi.org/10.1111/j.1471-4159.2009.06170.x.

43. L. Keller *et al.*, "The PSEN1 I143T mutation in a Swedish family with Alzheimer's disease: clinical report and quantification of Aβ in different brain regions," *European Journal of Human Genetics*, vol. 18, no. 11, pp. 1202–1208, 2010/11/01 2010, doi: 10.1038/ejhg.2010.107.

44. A. Sandebring, H. Welander, B. Winblad, C. Graff, and L. O. Tjernberg, "The pathogenic aβ43 is enriched in familial and sporadic Alzheimer disease," (in eng), *PLoS One*, vol. 8, no. 2, p. e55847, 2013, doi: 10.1371/journal.pone.0055847.

45. C. Lauridsen *et al.*, "Cerebrospinal Fluid Levels of Amyloid Beta 1–43 in Patients with Amnestic Mild Cognitive Impairment or Early Alzheimer's Disease: A 2-Year Follow-Up Study," (in eng), *Front Aging Neurosci*, vol. 8, p. 30, 2016, doi: 10.3389/fnagi.2016.00030.

46. M. Mullan *et al.*, "A pathogenic mutation for probable Alzheimer's disease in the APP gene at the N-terminus of beta-amyloid," (in eng), *Nat Genet*, vol. 1, no. 5, pp. 345-7, Aug 1992, doi: 10.1038/ng0892-345.

47. M. D. Tambini and L. D'Adamio, "Trem2 Splicing and Expression are Preserved in a Human Abeta-producing, Rat Knock-in Model of Trem2-R47H Alzheimer's Risk Variant," *Sci Rep*, vol. 10, no. 1, p. 4122, Mar 5 2020, doi: 10.1038/s41598-020-60800-1.

48. T. Yin, W. Yao, K. A. Norris, and L. D'Adamio, "A familial Danish dementia rat shows impaired presynaptic and postsynaptic glutamatergic transmission," (in eng), *J Biol Chem*, vol. 297, no. 3, p. 101089, 09 2021, doi: 10.1016/j.jbc.2021.101089.

49. R. Tamayev, S. Matsuda, M. Fà, O. Arancio, and L. D'Adamio, "Danish dementia mice suggest that loss of function and not the amyloid cascade causes synaptic plasticity and memory deficits," (in eng), *Proc Natl Acad Sci U S A*, vol. 107, no. 48, pp. 20822-7, Nov 2010, doi: 10.1073/pnas.1011689107.

50. S. Ren *et al.*, "TNF-α-mediated reduction in inhibitory neurotransmission precedes sporadic Alzheimer's disease pathology in young Trem2 R^{47H} rats," (in eng), *J Biol Chem*, vol. 296, p. 100089, Nov

2020, doi: 10.1074/jbc.RA120.016395.

51. S. Ren, W. Yao, M. D. Tambini, T. Yin, K. A. Norris, and L. D'Adamio, "Microglia *TREM2* ^{R47H} Alzheimer-linked variant enhances excitatory transmission and reduces LTP via increased TNF-α levels," (in eng), *Elife*, vol. 9, 06 2020, doi: 10.7554/eLife.57513.

Tables

Target	Antibody	Antigen retrieval	Dilution	Secondary & Amplification
Neurons	NeuN, Mouse monoclonal A60, Millipore	Citrate HIER	1:3000	RbaM & GtaRb-HRP
Amyloid b	1-16 and 17-24 Amyloid b Mouse monoclonal 6E10 and 4G8, Biolegend	80% Formic Acid	1:1000 1:1000	RbaM & GtaRb-HRP
Microglia	Iba1, Rabbit polyclonal, Wako	Citrate HIER	1:200	GtaCk-HRP
Astrocytes	GFAP, Rabbit polyclonal, Thermo Scientific	Citrate HIER	1:200	DkaRb-bio & SA-HRP
Phospho-tau	Phospho-tau , AT8, Mouse monoclonal, Thermo Scientific	Citrate HIER	1:1000	HaM-bio & SA-HRP
Abeta40	Amyloid Beta 40, Mouse monoclonal G2-10, Millipore	80% Formic Acid	1:500	HaM-bio & SA-HRP
Abeta42	Amyloid Beta 42, Mouse monoclonal G2-11, Millipore	80% Formic Acid	1:500	HaM-bio & SA-HRP
Abeta43	Amyloid Beta 43, Rabbit polyclonal, IBL-America	80% Formic Acid	1:100	DkaRb-bio & SA-HRP

Table 1. Primary and amplification antibodies used for IHC. ∝= anti; bio= biotin; Dk = Donkey; Gt = Goat; Ck = Chicken; HIER = Heat induced antigen retrieval; H=Horse; HRP= Horseradish Peroxidase; M = Mouse; Rb = Rabbit; SA=Streptavidin.

Groups	NeuN	Iba1	GFAP
$App^{h/h}$:$Psen1^{w/w}$	2.06±0.2	2.25±0.25	2.35±0.41
$App^{h/h}$:$Psen1^{LF/w}$	1.91±0.18	2.12±0.28	2.5±0.63
$App^{h/h}$:$Psen1^{LF/LF}$	1.70±0.22	2.2±0.3	1.83±0.37
$App^{s/h}$:$Psen1^{LF/LF}$	1.91±0.18	2.02±0.07	2.12±0.74
$App^{s/s}$:$Psen1^{LF/LF}$	2.05±0.5	2.35±0.34	2.06±0.46

Table 2. Qualitative Scoring of IHC. Summary of the qualitative assessment performed on the NeuN, Iba1 and GFAP IHC. Assessments were performed on a 0 to 3 scale (1=low, 2=average, 3=high), with 0.5 increments, on the dorsal hippocampus and the cortex above, the mean and the standard deviation are shown. No qualitative evaluation was performed in the P- Tau, AT8 samples due to the absence of staining, nor in the H&E and silver stains due to the lack of perceivable discriminative features.

Groups	Focal hippocampal neurodegeneration	Iba1 foci	Iba1 Activation region	Amyloid Plaques
$App^{h/h}$:$Psen1^{w/w}$	0/14 (0%)	0/14 (0%)	0/14 (0%)	0/14 (0%)
$App^{h/h}$:$Psen1^{LF/w}$	0/6 (0%)	1/6 (16.6%)	1/6 (16.6%)	0/6 (0%)
$App^{h/h}$:$Psen1^{LF/LF}$	0/6 (0%)	1/6 (16.6%)	1/6 (16.6%)	0/6 (0%)
$App^{s/h}$:$Psen1^{LF/LF}$	1/12 (8.3%)	3/12 (25%)	2/12 (16.6%)	2/12 (16.6%)
$App^{s/s}$:$Psen1^{LF/LF}$	1/10 (10%)	3/10 (30%)	2/10 (20%)	10/10 (100%)

Table 3. Summary of the pathological features observed in all the groups. Summary of the pathological features observed in all the groups studied, the frequency of occurrence is expressed as percentage.

Figures

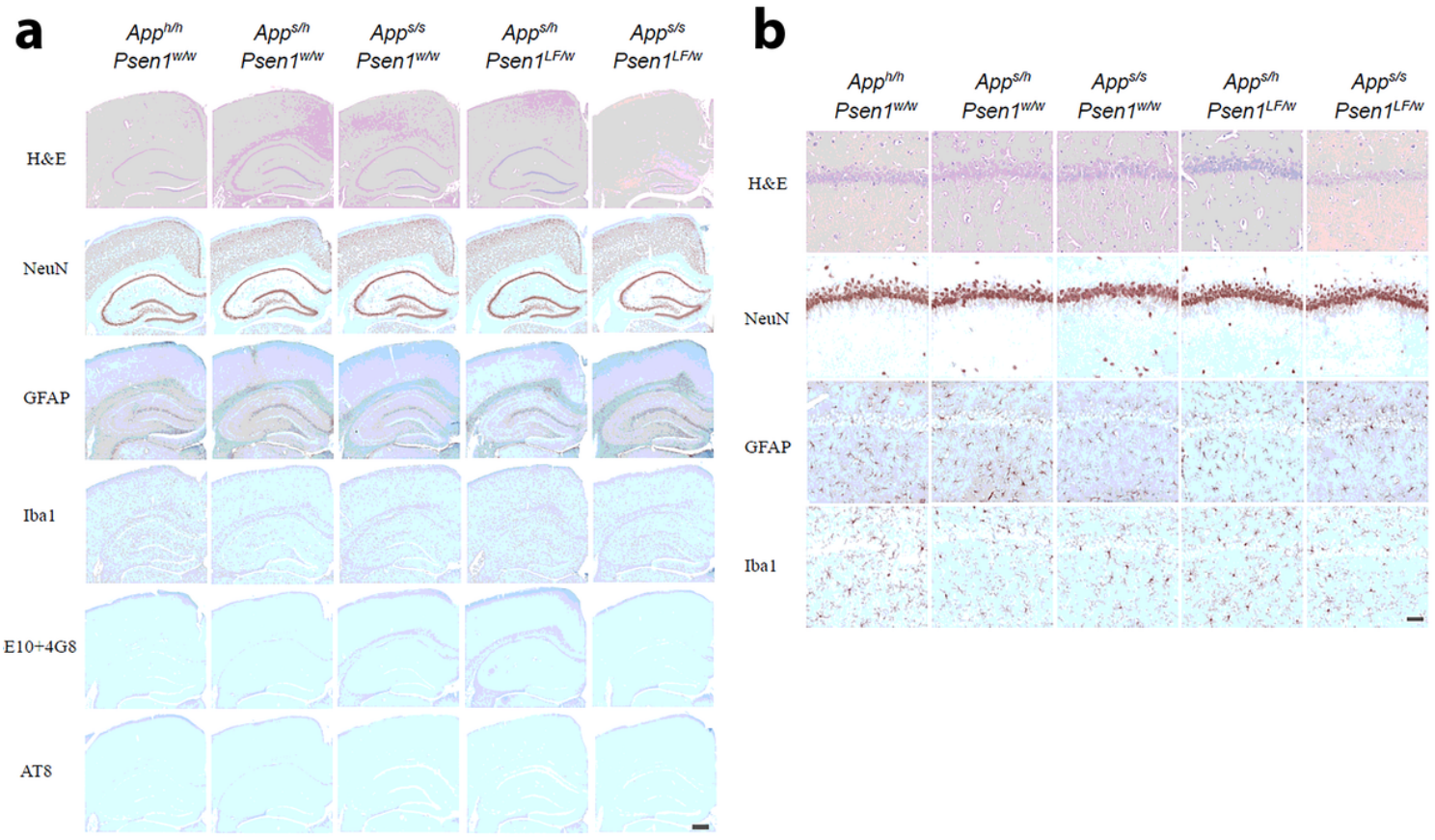

Figure 1

Histopathological analysis of 18-month-old KI rats with different combinations of *App* and *Psen1* mutant alleles. (**a**) Representative images of the anterior hippocampus and overlaying somatosensory cortex of rat brains. Illustrates of, from the top to bottom, NeuN, GFAP, Iba1, Amyloid-Beta (6E10+4G8) and phospho-Tau (AT8) staining, respectively. The scale bar is equivalent to 500 microns. (**b**) High-magnification picture of the hippocampal CA1 subregion for the samples depicted in (**a**). Illustrates of,

from the top to bottom, NeuN, GFAP, Iba1, Amyloid-Beta (6E10+4G8) and phospho-Tau (AT8) staining, respectively. The scale bar is equivalent to 50 microns.

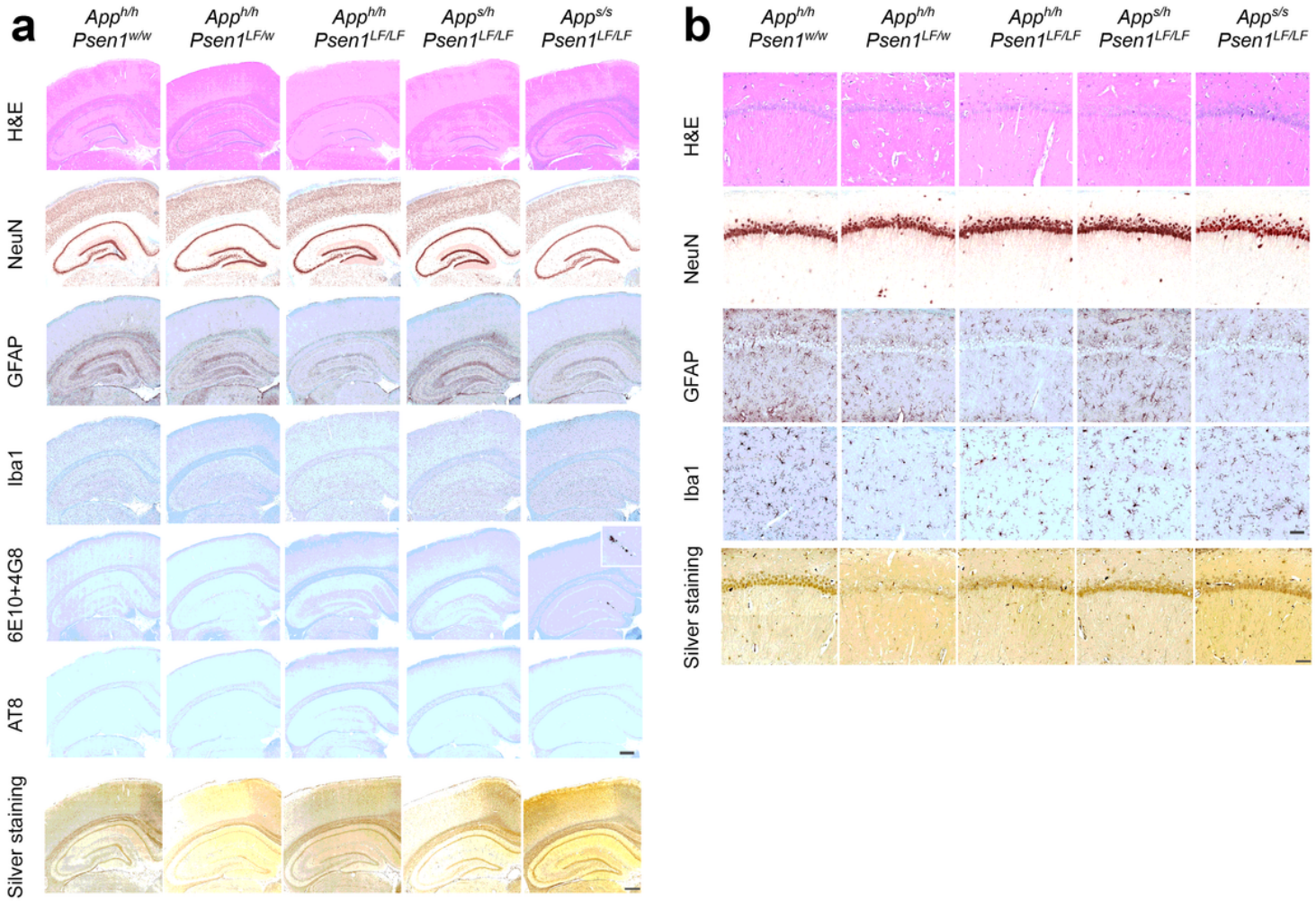

Figure 2

H&E, NeuN, GFAP, Iba1, 6E10 + 4G8 (Amyloid β), AT8 (pTau) and modified Bielshowski Silver staining of 14 month-old knock-in rats carrying *App*^{s} and *Psen1*^{LF} FAD mutations. Staining was performed in rats of the following genotypes (number of female and male rats used are indicated in parentheses): *App*$^{h/h}$*:Psen1*$^{w/w}$ (7 females and 7 males), *App*$^{h/h}$*:Psen1*$^{LF/w}$ (5 females and 1 males), *App*$^{h/h}$*:Psen1*$^{LF/LF}$ (2 females and 4 males), *App*$^{s/h}$*:Psen1*$^{LF/LF}$ (6 females and 6 males) and *App*$^{s/s}$*:Psen1*$^{LF/LF}$ (8 female and 2 males) knock-in rats. (**a**) Representative images in *App*$^{h/h}$*:Psen1*$^{w/w}$, *App*$^{h/h}$*:Psen1*$^{LF/w}$, *App*$^{h/h}$*:Psen1*$^{LF/LF}$, *App*$^{s/h}$*:Psen1*$^{LF/LF}$, and *App*$^{s/s}$*:Psen1*$^{LF/LF}$ rats are illustrated from left to right. The scale bar is equivalent to 500 microns. An insert the 6E10 + 4G8 *App*$^{s/s}$*:Psen1*$^{LF/LF}$ panel shows higher magnification of small hippocampus plaques. (**b**) Detailed images of the H&E, NeuN, GFAP, Iba1 and modified Bielshowski Silver staining in the dorsal hippocampus-CA1. The scale bar is equivalent to 50 microns.

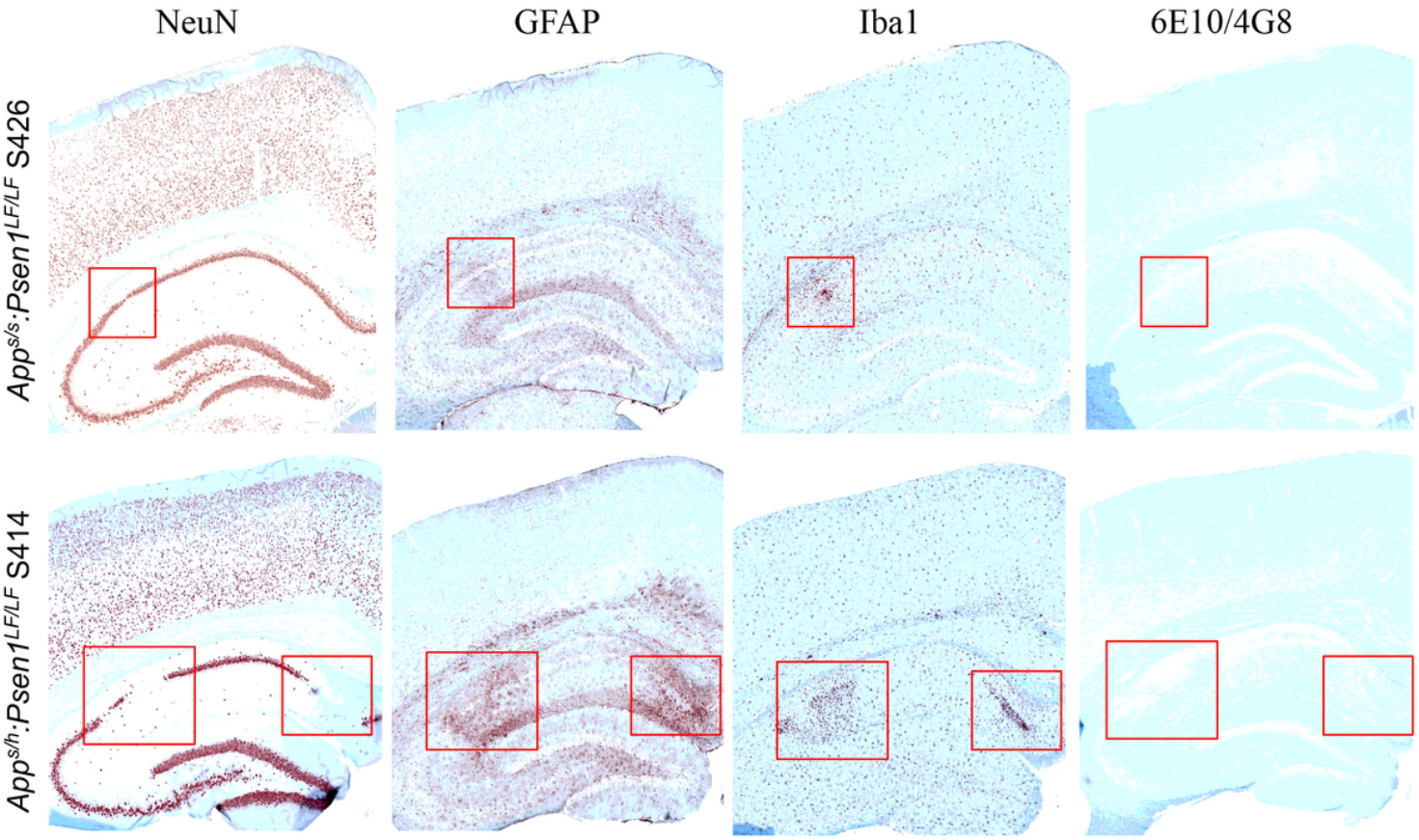

Figure 3

Representative pictures illustrating hippocampal neurodegeneration in two samples, *App*$^{s/s}$*:Psen1*$^{LF/LF}$ S426 and *App*$^{s/h}$*:Psen1*$^{LF/LF}$ S414. NeuN, GFAP, IBA1 and Amyloid staining performed on consecutive sections in *App*$^{s/s}$*:Psen1*$^{LF/LF}$ S426 and *App*$^{s/h}$*:Psen1*$^{LF/LF}$ S414. Area of neurodegeneration is shown with a square. The scale bar is equivalent to 500 microns.

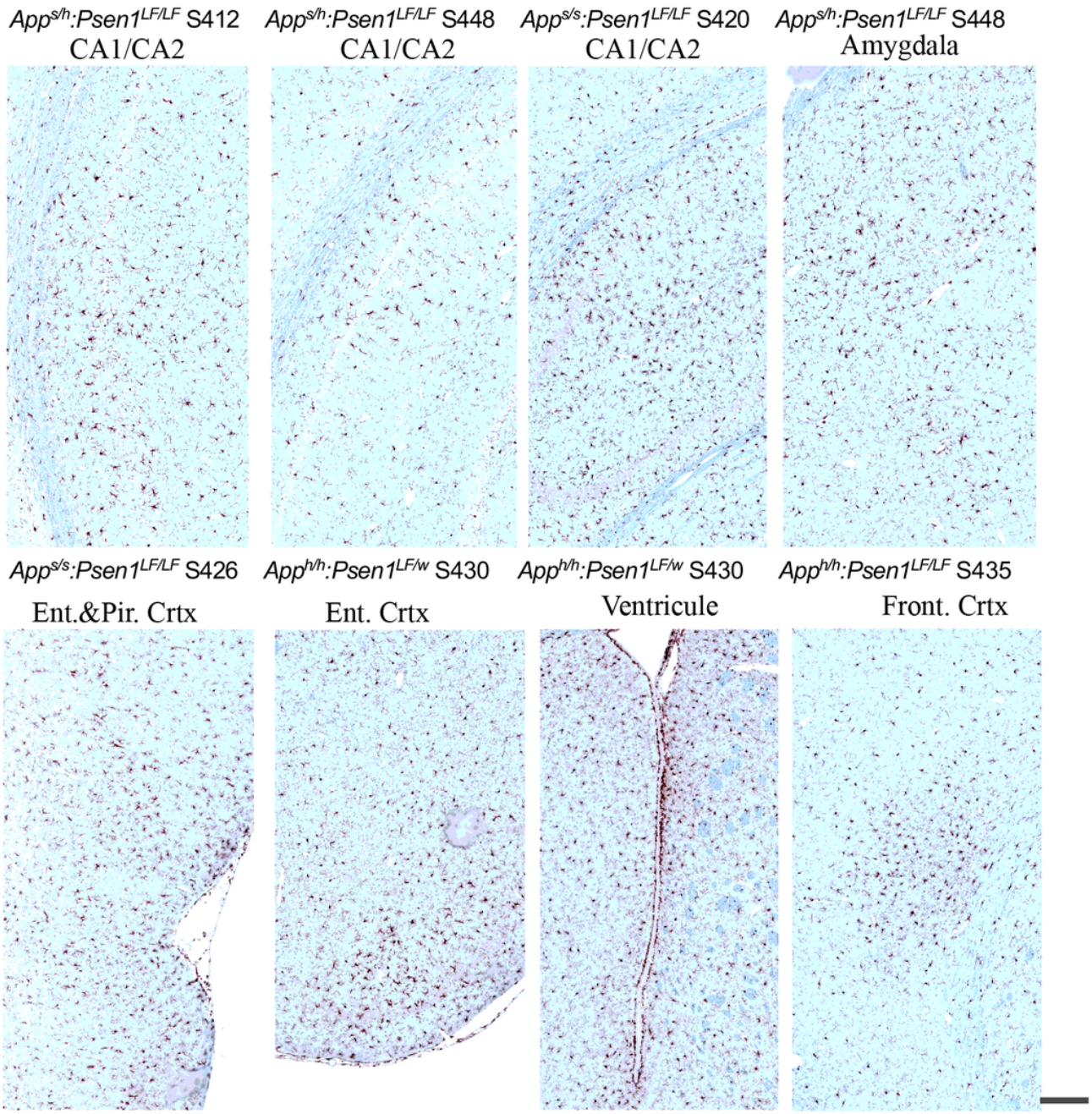

Figure 4

Representative areas with IBA1 microglial activation magnification in knock-in rats *App*$^{s/s}$*:Psen1*$^{LF/LF}$ S420 and S426, *App*$^{s/h}$*:Psen1*$^{LF/LF}$ S412, S448, *App*$^{h/h}$*:Psen1*$^{LF/w}$ S430 and *App*$^{h/h}$*:Psen1*$^{LF/LF}$ S435. Representative images of the IBA1 feature called “microglial activation” (red-brown chromogen) in knock-in rats. All pictures were taken at the same magnification, the scale bar is equivalent to 200 microns.

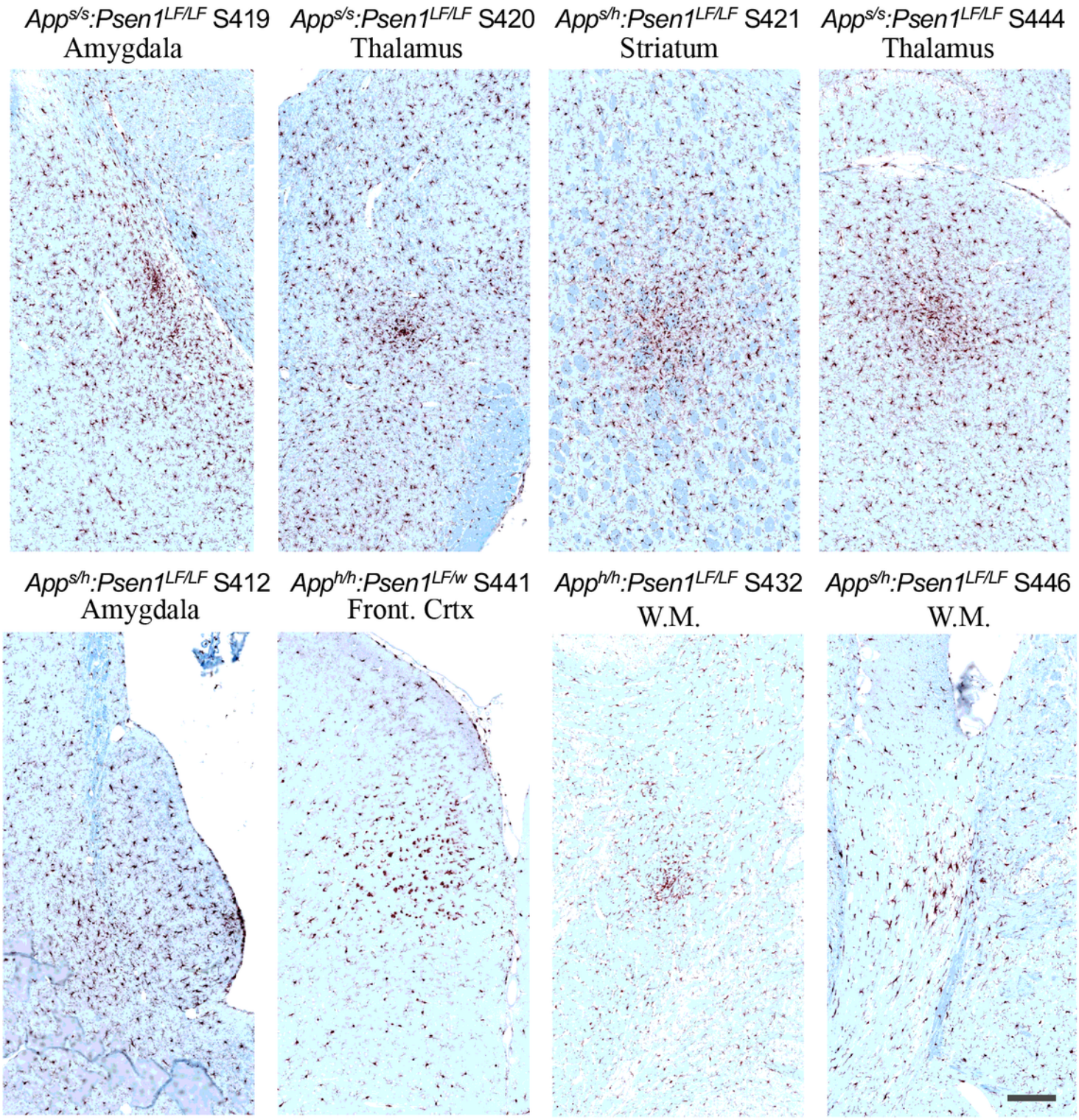

Figure 5

Representative IBA1 microglial foci magnification in knock-in rats *App*$^{s/s}$:*Psen1*$^{LF/LF}$ S419, S420 and S444, *App*$^{s/h}$:*Psen1*$^{LF/LF}$ S412, S421 and 446, *App*$^{h/h}$:*Psen1*$^{LF/w}$ S441 and *App*$^{h/h}$:*Psen1*$^{LF/LF}$ S432. Representative images of the IBA1 feature called “microglial foci” (red-brown chromogen) in knock-in rats. All pictures were taken at the same magnification, the scale bar is equivalent to 200 microns.

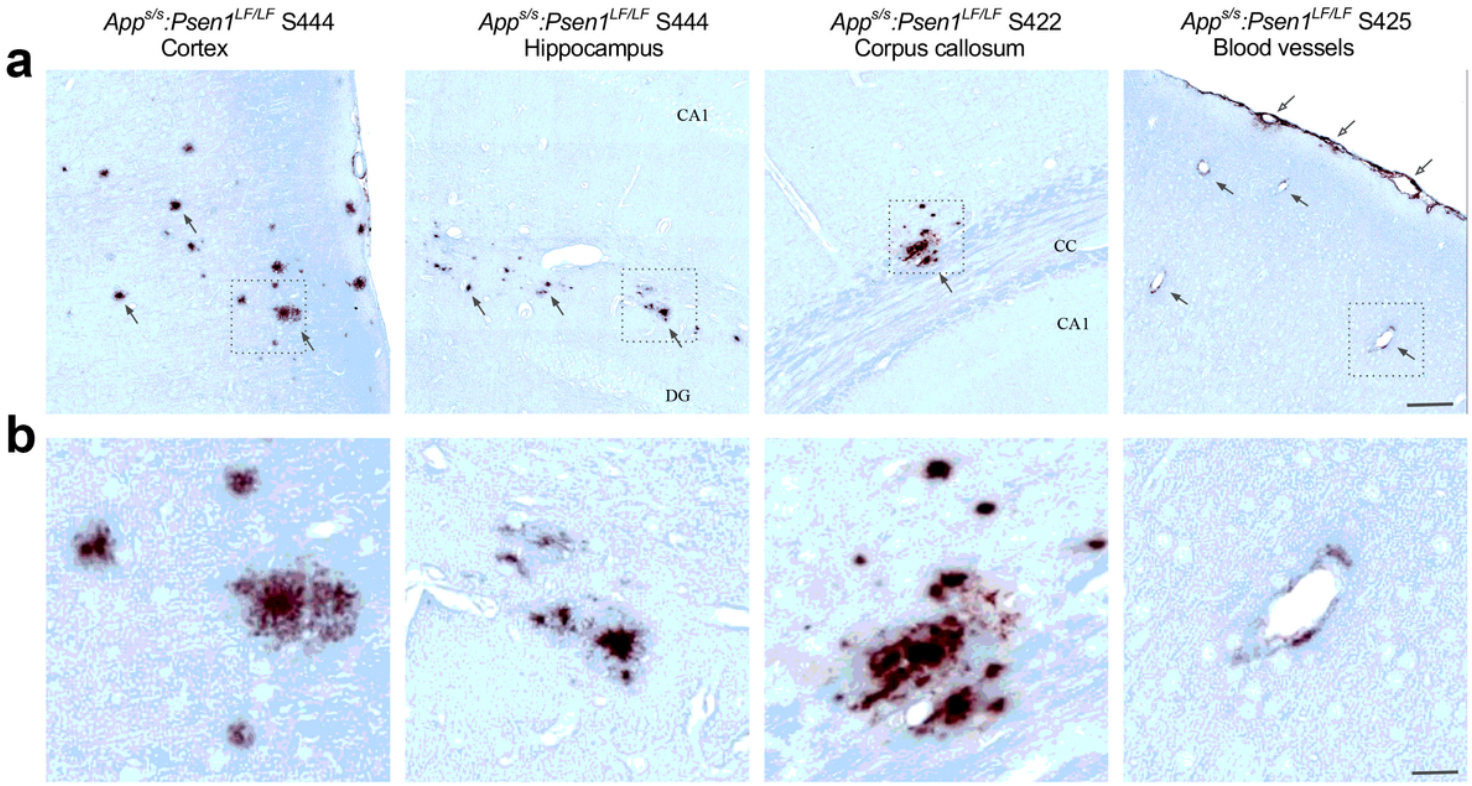

Figure 6

Amyloid deposition examples in the cortex, hippocampus, corpus callosum and blood vessels. (**a**) Representative staining of amyloid deposits, from left to right, in the cortex (*App*$^{s/s}$*:Psen1*$^{LF/LF}$ S444), the hippocampus (*App*$^{s/s}$*:Psen1*$^{LF/LF}$, S444), the corpus callosum (*App*$^{s/s}$*:Psen1*$^{LF/LF}$, S422) and blood vessels (*App*$^{s/s}$*:Psen1*$^{LF/LF}$, S425) (CA1: CA1 region of the hippocampus, DG: Dentate Gyrus, CC: Corpus Callosum). Squares indicate the area magnified in row (**a**), arrows indicate plaques or vessels deposit locations. Open arrows indicate leptomeningeal amyloid deposition. The scale bar is equivalent to 100 microns and 25 microns respectively.

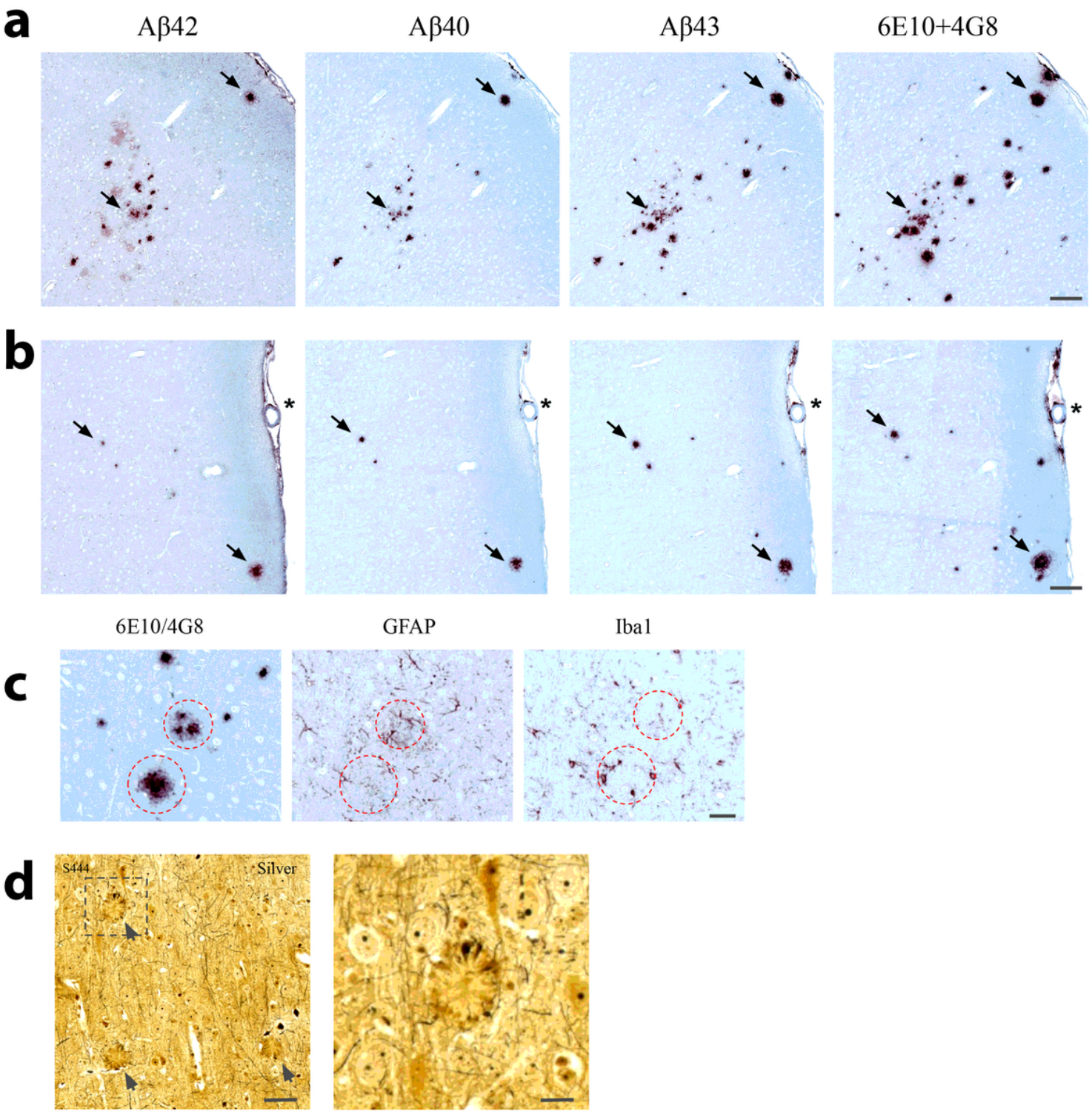

Figure 7

Characterization of amyloid plaques. Staining with Aβ42, Aβ40, Aβ43 and pan-Aβ antibodies Consecutive slides staining with Aβ42, Aβ40, Aβ43 and pan-Aβ (6E10/4G8 mix) in *App*$^{s/s}$*:Psen1*$^{LF/LF}$ S425 (**a**) and S444 (**b**) cortex. Dark arrows indicate amyloid plaques locations present on the 4 slides, note the presence of all the Aβ isoforms tested in the amyloid plaques. The asterisk in (**b**) indicates leptomeningeal amyloid deposition. Scale bar is equivalent to 100um. (**c**) IBA1 and GFAP staining in the

vicinity of amyloid plaques. Consecutive slides staining with 6E10/4G8, GFAP and Iba1 in a region of the cortex with amyloid deposits (*App*$^{s/s}$:*Psen1*$^{LF/LF}$ S450). The scale bar is equivalent to 25 microns. (**d**) Representative images of amyloid plaques stained with silver staining in *App*$^{s/s}$:*Psen1*$^{LF/LF}$ S444. Grey arrows indicate the amyloid plaques and the square is magnified on the right panel. The scale bar displayed is equivalent to 50 microns and 5 microns respectively.

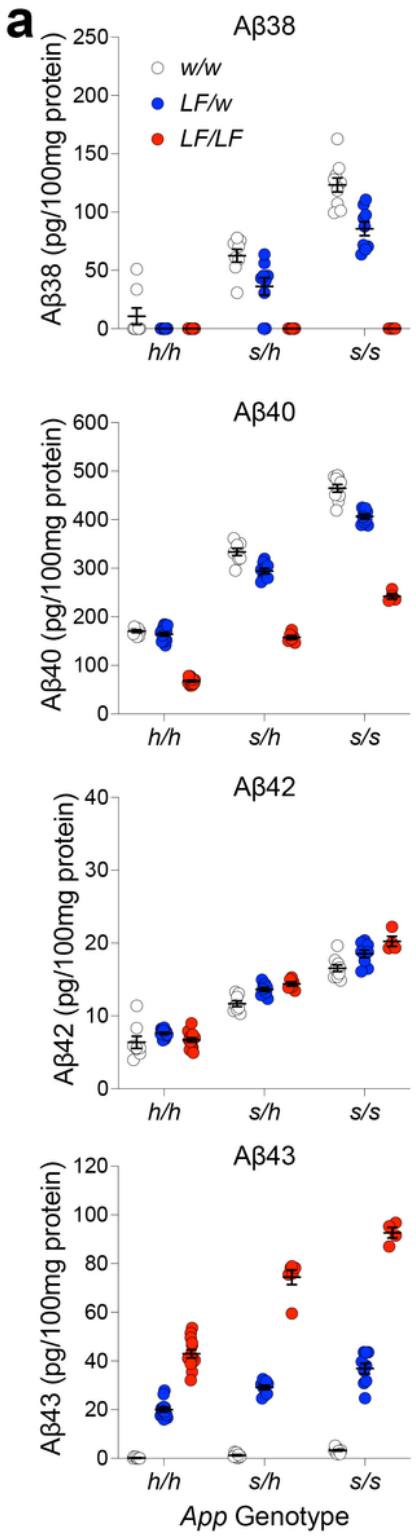

b

		Aβ38	Aβ40	Aβ42	Aβ43
Two-way ANOVA, Ordinary	Interaction	F (4, 73) = 32.14, P<0.0001	F (4, 73) = 31.28, P<0.0001	F (4, 73) = 4.129, P=0.0045	F (4, 73) = 61.85, P<0.0001
	App genotype Factor	F (2, 73) = 139.1, P<0.0001	F (2, 73) = 1562, P<0.0001	F (2, 73) = 537.0, P<0.0001	F (2, 73) = 185.9, P<0.0001
	Psen1 genotype Factor	F (2, 73) = 118.1, P<0.0001	F (2, 73) = 698.3, P<0.0001	F (2, 73) = 20.40, P<0.0001	F (2, 73) = 1314, P<0.0001
		Adjusted P Value	Adjusted P Value	Adjusted P Value	Adjusted P Value
Tukey's multiple compar. test	*h/h:w/w vs. h/h:LF/w*	0.7386	0.9915	0.3935	<0.0001
	h/h:w/w vs. h/h:LF/LF	0.7386	<0.0001	0.9997	<0.0001
	h/h:w/w vs. s/h:w/w	<0.0001	<0.0001	<0.0001	0.9999
	h/h:w/w vs. s/h:LF/w	0.0096	<0.0001	<0.0001	<0.0001
	h/h:w/w vs. s/h:LF/LF	0.8931	0.8362	<0.0001	<0.0001
	h/h:w/w vs. s/s:w/w	<0.0001	<0.0001	<0.0001	0.8519
	h/h:w/w vs. s/s:LF/w	<0.0001	<0.0001	<0.0001	<0.0001
	h/h:w/w vs. s/s:LF/LF	0.9453	<0.0001	<0.0001	<0.0001
	h/h:LF/w vs. h/h:LF/LF	>0.9999	<0.0001	0.5805	<0.0001
	h/h:LF/w vs. s/h:w/w	<0.0001	<0.0001	<0.0001	<0.0001
	h/h:LF/w vs. s/h:LF/w	<0.0001	<0.0001	<0.0001	0.0002
	h/h:LF/w vs. s/h:LF/LF	>0.9999	0.994	<0.0001	<0.0001
	h/h:LF/w vs. s/s:w/w	<0.0001	<0.0001	<0.0001	<0.0001
	h/h:LF/w vs. s/s:LF/w	<0.0001	<0.0001	<0.0001	<0.0001
	h/h:LF/w vs. s/s:LF/LF	>0.9999	<0.0001	<0.0001	<0.0001
	h/h:LF/LF vs. s/h:w/w	<0.0001	<0.0001	<0.0001	<0.0001
	h/h:LF/LF vs. s/h:LF/w	<0.0001	<0.0001	<0.0001	<0.0001
	h/h:LF/LF vs. s/h:LF/LF	>0.9999	<0.0001	<0.0001	<0.0001
	h/h:LF/LF vs. s/s:w/w	<0.0001	<0.0001	<0.0001	<0.0001
	h/h:LF/LF vs. s/s:LF/w	<0.0001	<0.0001	<0.0001	0.0434
	h/h:LF/LF vs. s/s:LF/LF	>0.9999	<0.0001	<0.0001	<0.0001
	s/h:w/w vs. s/h:LF/w	0.0065	<0.0001	0.0507	<0.0001
	s/h:w/w vs. s/h:LF/LF	<0.0001	<0.0001	0.0051	<0.0001
	s/h:w/w vs. s/s:w/w	<0.0001	<0.0001	<0.0001	0.9871
	s/h:w/w vs. s/s:LF/w	0.0287	<0.0001	<0.0001	<0.0001
	s/h:w/w vs. s/s:LF/LF	<0.0001	<0.0001	<0.0001	<0.0001
	s/h:LF/w vs. s/h:LF/LF	0.0002	<0.0001	0.9697	<0.0001
	s/h:LF/w vs. s/s:w/w	<0.0001	<0.0001	0.0001	<0.0001
	s/h:LF/w vs. s/s:LF/w	<0.0001	<0.0001	<0.0001	0.01
	s/h:LF/w vs. s/s:LF/LF	0.0016	<0.0001	<0.0001	<0.0001
	s/h:LF/LF vs. s/s:w/w	<0.0001	<0.0001	0.0347	<0.0001
	s/h:LF/LF vs. s/s:LF/w	<0.0001	<0.0001	<0.0001	<0.0001
	s/h:LF/LF vs. s/s:LF/LF	>0.9999	<0.0001	<0.0001	<0.0001
	s/s:w/w vs. s/s:LF/w	<0.0001	<0.0001	0.0277	<0.0001
	s/s:w/w vs. s/s:LF/LF	<0.0001	<0.0001	0.0002	<0.0001
	s/s:LF/w vs. s/s:LF/LF	<0.0001	<0.0001	0.3915	<0.0001

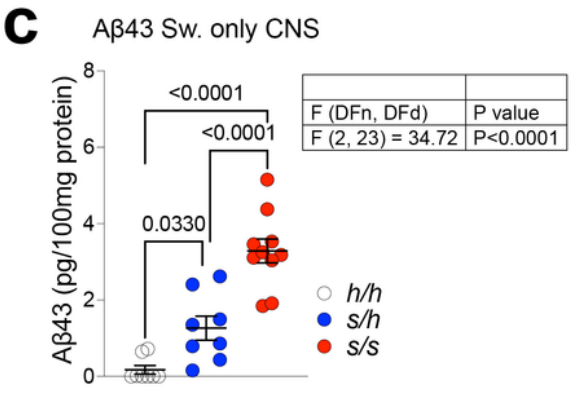

F (DFn, DFd)	P value
F (2, 23) = 34.72	P<0.0001

Figure 8

Levels of Aβ38, Aβ40, Aβ42 and Aβ43 in the CNS of 7 month-old knock-in rats carrying *App*^{s} and *Psen1*^{LF} FAD mutations. (**a**) Aβ38, Aβ40, Aβ42 and Aβ43 were measured in rats of the following genotypes (number of female and male rats used are indicated in parentheses): *App*$^{h/h}$*:Psen1*$^{w/w}$ (4 females and 4 males), *App*$^{s/h}$*:Psen1*$^{w/w}$ (4 females and 4 males), *App*$^{s/s}$*:Psen1*$^{w/w}$ (6 females and 4 males), *App*$^{h/h}$*:Psen1*$^{LF/w}$ (9 females and 5 males), *App*$^{s/h}$*:Psen1*$^{LF/w}$ (4 females and 5 males), *App*$^{s/s}$*:Psen1*$^{LF/w}$ (4 females and 5 males), *App*$^{h/h}$*:Psen1*$^{LF/LF}$ (5 females and 7 males), *App*$^{s/h}$*:Psen1*$^{LF/LF}$ (2 females and 2 males) and *App*$^{s/s}$*:Psen1*$^{LF/LF}$ (1 female and 3 males) knock-in rats. Data are represented as mean ± SEM and were analyzed by ordinary two-way ANOVA followed by ad hoc Tukey's multiple comparison test when ANOVA shows significant differences. Detailed statistical analysis is reported in (**b**), with significant difference reported in red. (**c**) Ordinary one-way ANOVA (F (2, 23) = 34.72, P<0.0001) and Tukey's multiple comparison test comparing Aβ43 levels of *App*$^{h/h}$*:Psen1*$^{w/w}$, *App*$^{s/h}$*:Psen1*$^{w/w}$ and *App*$^{s/s}$*:Psen1*$^{w/w}$ knock-in rats. The P values of the 3 comparisons are reported in the panel.

a

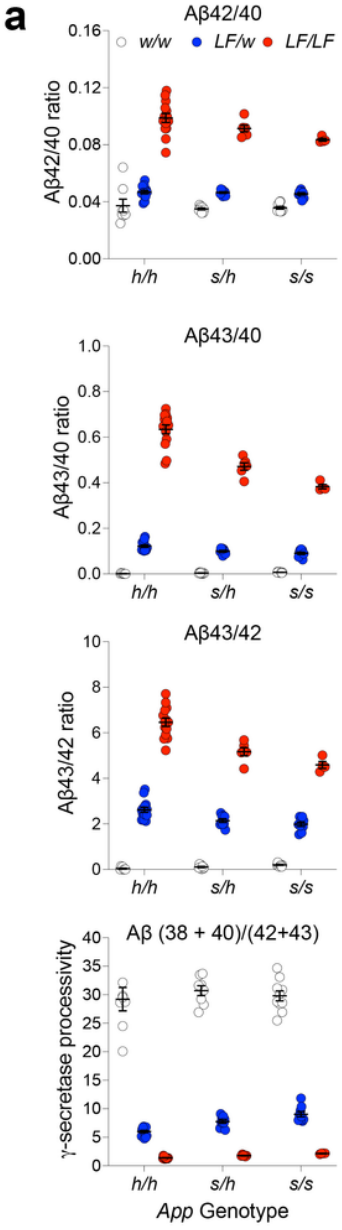

b

		Aβ42/40	Aβ43/40	Aβ43/42	Processivity
Two-way ANOVA, Ordinary	Interaction	F (4, 73) = 2.529, P=0.0477	F (4, 73) = 33.08, P<0.0001	F (4, 73) = 14.90, P<0.0001	F (4, 73) = 1.133, P=0.3477
	App genotype Factor	F (2, 73) = 4.806, P=0.0109	F (2, 73) = 48.52, P<0.0001	F (2, 73) = 29.82, P<0.0001	F (2, 73) = 3.238, P=0.0499
	Psen1 genotype Factor	F (2, 73) = 369.5, P<0.0001	F (2, 73) = 1166, P<0.0001	F (2, 73) = 1030, P<0.0001	F (2, 73) = 1017, P<0.0001
		Adjusted P Value	Adjusted P Value	Adjusted P Value	Adjusted P Value
Tukey's multiple compar. test	*h/h:w/w vs. h/h:LF/w*	0.0685	<0.0001	<0.0001	<0.0001
	h/h:w/w vs. h/h:LF/LF	<0.0001	<0.0001	<0.0001	<0.0001
	h/h:w/w vs. s/h:w/w	0.9992	>0.9999	>0.9999	0.9224
	h/h:w/w vs. s/h:LF/w	0.1618	<0.0001	<0.0001	<0.0001
	h/h:w/w vs. s/h:LF/LF	<0.0001	<0.0001	<0.0001	<0.0001
	h/h:w/w vs. s/s:w/w	>0.9999	>0.9999	0.9916	0.9998
	h/h:w/w vs. s/s:LF/w	0.2735	<0.0001	<0.0001	<0.0001
	h/h:w/w vs. s/s:LF/LF	<0.0001	<0.0001	<0.0001	<0.0001
	h/h:LF/w vs. h/h:LF/LF	<0.0001	<0.0001	<0.0001	<0.0001
	h/h:LF/w vs. s/h:w/w	0.0084	<0.0001	<0.0001	<0.0001
	h/h:LF/w vs. s/h:LF/w	>0.9999	0.8416	0.1015	0.6889
	h/h:LF/w vs. s/h:LF/LF	<0.0001	<0.0001	<0.0001	0.0083
	h/h:LF/w vs. s/s:w/w	0.0075	<0.0001	<0.0001	<0.0001
	h/h:LF/w vs. s/s:LF/w	>0.9999	0.4685	0.0063	0.0622
	h/h:LF/w vs. s/s:LF/LF	<0.0001	<0.0001	<0.0001	0.083
	h/h:LF/LF vs. s/h:w/w	<0.0001	<0.0001	<0.0001	<0.0001
	h/h:LF/LF vs. s/h:LF/w	<0.0001	<0.0001	<0.0001	<0.0001
	h/h:LF/LF vs. s/h:LF/LF	0.433	<0.0001	<0.0001	>0.9999
	h/h:LF/LF vs. s/s:w/w	<0.0001	<0.0001	<0.0001	<0.0001
	h/h:LF/LF vs. s/s:LF/w	<0.0001	<0.0001	<0.0001	<0.0001
	h/h:LF/LF vs. s/s:LF/LF	0.0069	<0.0001	<0.0001	0.9996
	s/h:w/w vs. s/h:LF/w	0.0304	<0.0001	<0.0001	<0.0001
	s/h:w/w vs. s/h:LF/LF	<0.0001	<0.0001	<0.0001	<0.0001
	s/h:w/w vs. s/s:w/w	>0.9999	>0.9999	>0.9999	0.9949
	s/h:w/w vs. s/s:LF/w	0.0618	<0.0001	<0.0001	<0.0001
	s/h:w/w vs. s/s:LF/LF	<0.0001	<0.0001	<0.0001	<0.0001
	s/h:LF/w vs. s/h:LF/LF	<0.0001	<0.0001	<0.0001	0.0001
	s/h:LF/w vs. s/s:w/w	0.0318	<0.0001	<0.0001	<0.0001
	s/h:LF/w vs. s/s:LF/w	>0.9999	0.9998	0.993	0.954
	s/h:LF/w vs. s/s:LF/LF	<0.0001	<0.0001	<0.0001	0.0032
	s/h:LF/LF vs. s/s:w/w	<0.0001	<0.0001	<0.0001	<0.0001
	s/h:LF/LF vs. s/s:LF/w	<0.0001	<0.0001	<0.0001	<0.0001
	s/h:LF/LF vs. s/s:LF/LF	0.7124	0.0051	0.3279	>0.9999
	s/s:w/w vs. s/s:LF/w	0.0669	<0.0001	<0.0001	<0.0001
	s/s:w/w vs. s/s:LF/LF	<0.0001	<0.0001	<0.0001	<0.0001
	s/s:LF/w vs. s/s:LF/LF	<0.0001	<0.0001	<0.0001	0.0001

Figure 9

Aβ42/Aβ40 ratios, Aβ43/Aβ40 ratios, Aβ43/Aβ42 ratios and γ-secretase processivity -(Aβ (38 + 40)/(42 + 43) ratios- in the CNS of 7 month-old knock-in rats carrying *App*^{s} and *Psen1*^{LF} FAD mutations. (**a**) Aβ42/Aβ40 ratios, Aβ43/Aβ40 ratios, Aβ43/Aβ42 ratios and γ-secretase processivity -(Aβ (38 + 40)/(42 + 43) ratios- were measured using the data shown in Fig. 2a. Data are represented as mean ± SEM and were analyzed by ordinary two-way ANOVA followed by ad hoc Tukey's multiple comparison test when ANOVA shows significant differences. Detailed statistical analysis is reported in (**b**), with significant difference reported in red.